

AD-A248 045



2

E 20920

PL-TR-91-2277

Laboratory Particle Velocity Experiments on Indiana Limestone and Sierra White Granite

S. A. Miller
A. L. Florence

SRI International
333 Ravenswood Avenue
Menlo Park, CA 94025-3493

October 1991

Final Report
5 October 1990 - January 1992

DTIC
SELECTE
MAR 10 1992
S D

Approved for public release; distribution unlimited



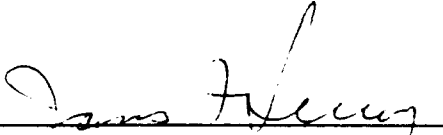
PHILLIPS LABORATORY
AIR FORCE SYSTEMS COMMAND
HANSCOM AIR FORCE BASE, MASSACHUSETTS 01731-5000

92-06134

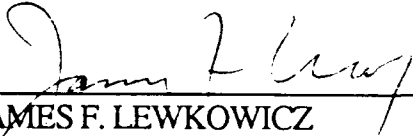


The views and conclusions contained in this document are those of the authors and should not be interpreted as representing the official policies, either expressed or implied, of the Air Force or the U.S. Government.


This technical report has been reviewed and is approved for publication.



JAMES F. LEWKOWICZ
Contract Manager
Solid Earth Geophysics Branch
Earth Sciences Division



JAMES F. LEWKOWICZ
Branch Chief
Solid Earth Geophysics Branch
Earth Sciences Division



DONALD H. ECKHARDT, Director
Earth Sciences Division

This document has been reviewed by the ESD Public Affairs Office (PA) and is releasable to the National Technical Information Service (NTIS).

Qualified requestors may obtain additional copies from the Defense Technical Information Center. All others should apply to the National Technical Information Service.

If your address has changed, or if you wish to be removed from the mailing list, or if the addressee is no longer employed by your organization, please notify PL/IMA, Hanscom AFB MA 01731-5000. This will assist us in maintaining a current mailing list.

Do not return copies of this report unless contractual obligations or notices on a specific document requires that it be returned.

REPORT DOCUMENTATION PAGE			Form Approved OMB No. 0704-0188		
Public reporting burden for this collection of information is estimated to average 1 hour per response, including the time for reviewing instructions, searching existing data sources, gathering and maintaining the data needed, and completing and reviewing the collection of information. Send comments regarding this burden estimate or any other aspect of this collection of information, including suggestions for reducing this burden, to Washington Headquarters Services, Directorate for Information Operations and Reports, 1215 Jefferson Davis Highway, Suite 1204, Arlington, VA 22202-4302, and to the Office of Management and Budget, Paperwork Reduction Project (0704-0188), Washington, DC 20503.					
1. AGENCY USE ONLY (Leave blank)	2. REPORT DATE October 1991	3. REPORT TYPE AND DATES COVERED Final - 90/10/05 - 02/01			
4. TITLE AND SUBTITLE LABORATORY PARTICLE VELOCITY EXPERIMENTS ON INDIANA LIMESTONE AND SIERRA WHITE GRANITE			5. FUNDING NUMBERS Contract: F19628-91-K-0003 PE 62101F, PE 61102F PR 7600 TA 09 WUAS		
6. AUTHOR(S) Miller, S. A. and Florence, A. L.					
7. PERFORMING ORGANIZATION NAME(S) AND ADDRESS(ES) SRI International 333 Ravenswood Avenue Menlo Park, CA 94025-3493			8. PERFORMING ORGANIZATION REPORT NUMBER SRI Project 1676		
9. SPONSORING/MONITORING AGENCY NAME(S) AND ADDRESS(ES) Phillips Laboratory/GPEH Hanscom Air Force Base, MA 01731-5000 Contact Manager: James F. Lewkowicz/GEH			10. SPONSORING/MONITORING AGENCY REPORT NUMBER PL-TR-91-2277		
11. SUPPLEMENTARY NOTES					
12a. DISTRIBUTION/AVAILABILITY STATEMENT Approved for public release; distribution unlimited.			12b. DISTRIBUTION CODE		
13. ABSTRACT (Maximum 200 words) Laboratory experiments were performed to determine the influence of freezing on the spherical wave generated by a small spherical explosive charge in rock. The work is relevant to the Soviet nuclear test site in Novaya Zemlya where permafrost conditions exist. The results are also valuable for developing and validating material modeling in continuum mechanics codes used for source coupling calculations. The experiments were performed with cores of well characterized Indiana limestone (porosity 16%) under frozen/dry and frozen/saturated conditions and well characterized Sierra White granite (porosity 0.8%) in a frozen/saturated condition. The spherical waves were determined by particle velocity measurements at several ranges. The effect of freezing was evaluated by comparing these results with results from our past room temperature experiments with the same <p style="text-align: right;">(over)</p>					
14. SUBJECT TERMS Indiana limestone Sierra White granite Dry, saturated, frozen			15. NUMBER OF PAGES 76		
			16. PRICE CODE		
17. SECURITY CLASSIFICATION OF REPORT UNCLASSIFIED			18. SECURITY CLASSIFICATION OF THIS PAGE UNCLASSIFIED	19. SECURITY CLASSIFICATION OF ABSTRACT UNCLASSIFIED	20. LIMITATION OF ABSTRACT SAR

UNCLASSIFIED

SECURITY CLASSIFICATION OF THIS PAGE


CLASSIFIED BY:

DECLASSIFY ON:

13. ABSTRACT (Continued)

rock type. From the particle velocities, we obtained displacements, reduced velocity and displacement potentials, spectra of these quantities, and radiated kinetic energy.

The main conclusions are that freezing the dry limestone and the saturated granited had no effect on the spherical waves. However, freezing of the saturated limestone had a substantial effect on the spherical waves. These effects included an increase of wave speed and reductions of maximum outward velocity, inward and outward phase durations, and displacements.

Accession For	
NTIS GRA&I	<input checked="" type="checkbox"/>
DTIC TAB	<input type="checkbox"/>
Unannounced	<input type="checkbox"/>
Justification	
By _____	
Distribution/	
Availability Codes	
Dist	Avail and/or Special
	



SECURITY CLASSIFICATION OF THIS PAGE

UNCLASSIFIED

SUMMARY

Laboratory experiments were performed to determine the influence of freezing on the spherical wave generated by a spherical explosive charge in rock. The work is relevant to the Soviet nuclear test site in Novaya Zemlya where permafrost conditions exist. The results are also valuable for developing and validating material modeling in continuum mechanics codes used for source coupling calculations.

In the experiments, the rock specimens consisted of cylinders 27 cm in diameter and 27 cm high of well characterized Indiana limestone and Sierra White granite. The wave source was a 1-cm-diameter sphere containing 3/8 gram of PETN powder packed to a density of 1.0 gram/cm³ (detonation pressure of 8.2 GPa). Particle velocity histories were measured at nine ranges using concentric copper loops placed in machined grooves along the midplane of the rock specimen. A constant axial magnetic field was applied to the specimen, and the particle velocity was measured by monitoring the induced voltage generated by each loop as it moved through the magnetic field. The velocity is the product of the induced voltage, the loop length, and the magnetic field strength according to Faraday's law.

The Indiana limestone, which had a porosity of 16%, was frozen (-8°C) under dry and saturated conditions. The Sierra White granite, which had a porosity of 0.8%, was frozen in a saturated condition. Wave results from our past experiments on those rocks at room temperature were used to assess the influence of freezing on the wave forms.

The experimental results showed that freezing affected the wave only in the Indiana limestone in a saturated condition. The main effects on the wave characteristics caused by freezing of the saturated Indiana limestone are as follows:

- (1) The wave speed increased from 4.7 mm/μs to 5.6 mm/μs.
- (2) The peak particle velocity decreased by about 10%, the outward and inward velocity phases shortened by about 30%, and a precursor wave appeared at the short ranges.
- (3) The maximum and final radial displacements were reduced by about 30%.
- (4) The reduced velocity potential maintained its maximum value, but the phase was reduced by about 30%.

- (5) The reduced displacement potential decreased by about 50%.
- (6) The low frequency content of the velocity spectrum decreased by about a factor of 2. The corner frequency increased (30 to 50 kHz), but the decay of the high frequency content showed little change. Similar changes occurred for the spectra of the displacements and potentials.
- (7) The radiated kinetic energy remained the same.

We recommend that similar experiments be performed in limestone of lower porosity to determine the trend of the influence and possibly to be more representative of the rock at Novaya Zemlya.

PREFACE

This research was conducted under Contract F19628-91-K-0003 sponsored by the Phillips Laboratory of the Air Force Systems Command. The technical monitor was Mr. James F. Lewkowicz.

The authors are indebted to the following personnel at SRI International who contributed to the program: E.M. Oyola for preparation and performance of the experiments, M.A. Merritt for instrumentation, and I.C. Adams for rock machining.

This research draws on results from two previous contracts on Indiana limestone (Contract DNA 001-90-C-0131) and Sierra White granite (Contract F19628-88-K-0051).

TABLE OF CONTENTS

Section	Page
SUMMARY	iii
PREFACE	v
LIST OF ILLUSTRATIONS	viii
LIST OF TABLES	ix
1 INTRODUCTION	1
2 DESCRIPTION OF EXPERIMENTS	2
2.1 Technique and Configuration	2
2.2 Rock Properties	4
2.3 Experiments Performed	4
3 EXPERIMENTAL RESULTS	10
3.1 Indiana Limestone Results	10
3.1.1 Particle Velocity	10
3.1.2 Displacement	13
3.1.3 Reduced Velocity Potential (RVP)	13
3.1.4 Reduced Displacement Potential (RDP)	13
3.1.5 Additional Results	13
3.2 Sierra White Granite Results	20
4 COMPARISON OF EXPERIMENTAL RESULTS	27
4.1 Indiana Limestone	27
4.1.1 Particle Velocity	27
4.1.2 Displacement	29
4.1.3 RVP and RDP	29
4.1.4 Spectra	29
4.1.5 Other Comparison	29
4.2 Sierra White Granite	38
5 CONCLUSIONS AND RECOMMENDATIONS	47
REFERENCES	48

TABLE OF CONTENTS (CONTINUED)

Section	Page
APPENDICES	
A OTHER EXPERIMENTAL RESULTS	A-1
B DEFINITIONS AND FORMULAS	B-1

LIST OF ILLUSTRATIONS

Figure		Page
1	Configuration of particle velocity experiments in Indiana limestone and Sierra White granite	3
2	Particle velocity histories measured at nine ranges in dry/frozen Indiana limestone, Test 598	11
3	Particle velocity histories measured at nine ranges in saturated/frozen Indiana limestone, Test 602	12
4	Displacement histories measured at nine ranges in dry/frozen Indiana limestone, Test 598	14
5	Displacement histories measured at nine ranges in saturated/frozen Indiana limestone, Test 602	15
6	Reduced velocity potential histories measured in dry/frozen Indiana limestone, Test 598	16
7	Reduced velocity potentials measured in saturated/frozen Indiana limestone, Test 602	17
8	Reduced displacement potentials measured in dry/frozen Indiana limestone, Test 598	18
9	Reduced displacement potentials measured in saturated/frozen Indiana limestone, Test 602	19
10	Particle velocity histories measured at eight ranges in saturated/frozen Sierra White granite, Test 591	21
11	Displacement histories measured at eight ranges in saturated/frozen Sierra White granite, Test 591	22
12	Reduced velocity potential histories measured in saturated/frozen Sierra White granite, Test 591	23
13	Reduced displacement histories measured in saturated/frozen Sierra White granite, Test 591	24
14	Velocity spectra measured at 25-mm range in saturated/frozen Sierra White granite, Test 591	25

LIST OF ILLUSTRATIONS (CONTINUED)

Figure		Page
15	Displacement spectra ($\xi - \xi_\infty$) measured at 25-mm range in saturated/frozen Sierra White granite, Test 591	25
16	Reduced velocity potential spectra measured at 25-mm range in saturated/frozen Sierra White granite, Test 591	26
17	Reduced displacement potential spectra ($\psi - \psi_\infty$) measured at 25-mm range in saturated/frozen Sierra White granite	26
18	Comparison of velocity histories at 30-mm range in Indiana limestone (16% porosity) for three different pore conditions	28
19	Comparison of displacement histories at 30-mm range in Indiana limestone (16% porosity) for three different pore conditions	30
20	Comparison of reduced velocity potential histories at 30-mm range in Indiana limestone (16% porosity) for three different pore conditions	31
21	Comparison of reduced displacement potential histories at 30-mm range in Indiana limestone (16% porosity) with three different pore conditions	32
22	Comparison of velocity spectra at the 30-mm range in Indiana limestone (16% porosity) with three different pore conditions	33
23	Comparison of displacement spectra at the 30-mm range in Indiana limestone (16% porosity) with three different pore conditions	34
24	Comparison of reduced velocity potential spectra at the 30-mm range in Indiana limestone (16% porosity) with three different pore conditions	35
25	Comparison of reduced displacement potential spectra at the 30-mm range in Indiana limestone (16% porosity) with three different pore conditions	36
26	Wavefront histories measured in Indiana limestone (16% porosity) for three different pore conditions	37
27	Attenuation of peak particle velocity in dry/frozen, saturated, and saturated/frozen Indiana limestone	39

LIST OF ILLUSTRATIONS (CONCLUDED)

Figure		Page
28	Attenuation of peak displacement measured in dry/frozen, saturated, and saturated/frozen Indiana limestone	41
29	Comparison of velocity attenuation in Sierra White granite with different pore conditions	44
30	Comparison of displacement attenuation in Sierra White granite with different pore conditions	44
A1	Particle velocity histories measured at nine ranges in saturated/frozen Indiana limestone, Test 600	A-2
A2	Particle velocity histories measured at nine ranges in saturated/frozen Indiana limestone, Test 605	A-3
A3	Comparison of velocity histories at 30-mm range in three experiments in saturated/frozen Indiana limestone	A-4
A4	Comparison of displacements at nine ranges from two experiments in saturated/frozen Indiana limestone	A-5
A5	Comparison of velocity histories at different ranges from two experiments in saturated/frozen Sierra White granite	A-6

LIST OF TABLES

Table		Page
1	Properties of Indiana limestone	5
2	Properties of Sierra White granite	6
3	Spherical wave experiments performed with frozen rock	7
4	Room temperature spherical wave results used for comparisons	9
5	Maximum particle velocities in Indiana limestone (m/s)	40
6	Maximum displacements in Indiana limestone (μm)	42
7	Radiated kinetic energy in Indiana limestone (J)	43
8	Maximum particle velocities in Sierra White granite (m/s)	45
9	Maximum displacements in Sierra White granite (μm)	46

SECTION 1

INTRODUCTION

Laboratory experiments were performed to determine the influence of freezing on the spherical wave generated by a small spherical explosive charge in rock. The work is relevant to the Soviet nuclear test site in Novaya Zemlya where permafrost conditions exist. The results are also valuable for developing and validating material modeling in continuum mechanics codes used for source coupling calculations.

Five experiments were performed with cores of well characterized Indiana limestone: two under frozen/dry conditions and three under frozen/saturated conditions. Three experiments were performed with cores of well characterized Sierra White granite under frozen/saturated conditions. Measurements of the spherical wave propagating from the spherical charge consisted of particle velocities at nine ranges. Rock properties and a description of the experimental technique are contained in Section 2. Wave results from our past experiments with identical Indiana limestone and Sierra White granite performed at room temperature were used to assess the influence of freezing on the wave forms. The frozen rock results are presented in Section 3 and comparisons with the corresponding room temperature results are made in Section 4. One test of each type was selected to describe the results and make the comparisons. The results of the repeat tests are given in Appendix A. Definitions and formulas used to process the data are given in Appendix B.

The main general conclusions are that freezing dry Indiana limestone and freezing dry and saturated Sierra White granite (porosity 0.8%) had almost no effect on the spherical waves. However, freezing of saturated Indiana limestone (porosity 16%) had a substantial effect on the spherical waves. The specific effects are listed in Section 5.

SECTION 2

DESCRIPTION OF EXPERIMENTS

2.1 TECHNIQUE AND CONFIGURATION

Figure 1 shows the main features of the technique and configuration of the rock experiments. A core of rock nominally 27 cm in diameter and height is cut into two equal cylinders, and the cut faces that will be brought together later are ground and smoothed flat. Hemispherical cavities are milled at the center of each of these faces for the spherical charge, which has a diameter of 1 cm. In the lower smooth face, nine concentric circular grooves, 0.254 mm wide and 0.381 mm deep, are milled with the radii shown in Figure 1(b). Annealed insulated copper wire of 0.229 mm diameter is epoxied into each circular groove and brought outside the rock specimen by a radial groove to form an electric circuit. The copper wire circles are the particle velocity gages. The charge is detonated by 2 grain/foot mild detonating fuse (MDF) contained in a stainless steel tube located in a hole drilled on axis in the upper rock cylinder. Gas dynamic calculations show that negligible venting of the cavity gases occurs during the velocity measurement period of the experiment. The spherical charge consists of 3/8 gram PETN powder packed to a density of 1 gram/cm³. The Chapman-Jouguet pressure is about 8 GPa. The explosive is contained in a spherical shell of Lucite with an outside diameter of 1 cm and a wall thickness of 0.5 mm. Before the testing, the two halves of the rock specimen are brought firmly together and cemented around the perimeter.

The assembled cylindrical specimen is lowered into a solenoid with a nominal diameter and height of 30 cm situated inside a pressure vessel. When overburden is required, the vessel is filled with fluid and pressurized. When dry rock is subjected to an overburden pressure, the specimen is given a thick coat of impermeable urethane.

The sequence of operations consists of applying the overburden pressure, turning on the solenoid current to create an axial magnetic field in the rock specimen, and detonating the charge. The wire loops expand at the particle velocity of the spherical wave generated by the charge. This velocity is obtained by Faraday's law; the voltage measured for a loop is equal to the product of the magnetic field strength, the loop length, and the wire velocity.

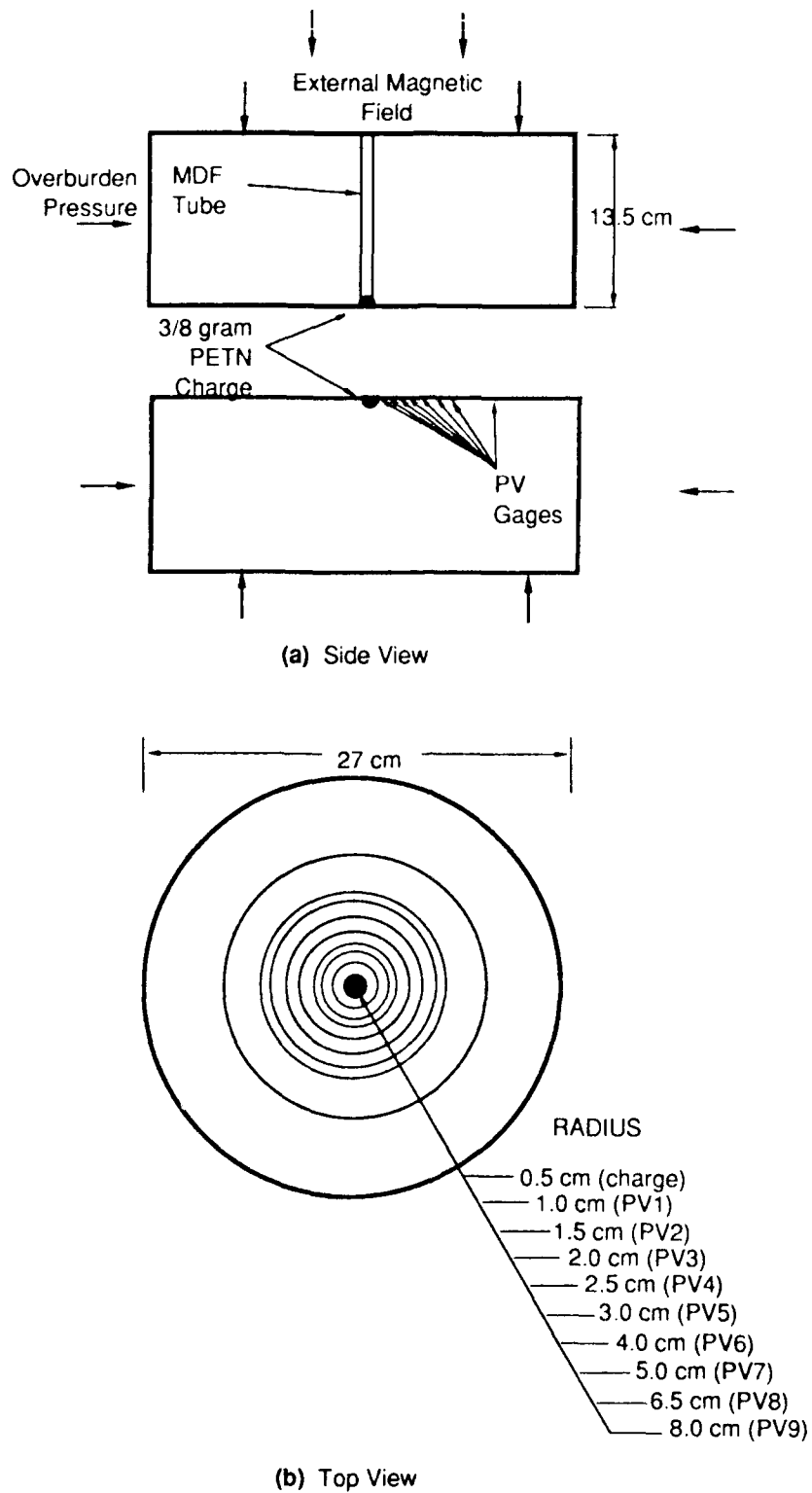


Figure 1 Configuration of particle velocity experiments in Indiana limestone and Sierra White granite.

To provide a frozen saturated state, we first subjected each half specimen to a vacuum on one flat face and deionized water on the other faces pressurized to 6.9 MPa. This process was performed in an apparatus specially designed for this purpose. The deionized water was compressed by a flatjack to prevent air from becoming entrained in the water. The saturation process was in place for 24 hours. Once fully saturated, the half specimens were placed in a freezer and kept at -20°C for at least 24 hours. The freezing process was designed to start at the lower flat surface and end at the upper flat surface by having an arrangement of insulation around the cylindrical side and on the flat top surface. This process prevents freezing from occurring first in the outside layers and progressing inward to cause a large buildup of pore pressure as the water expands as it freezes. This pressure either inhibits internal freezing or cracks the specimen. Freezing from the bottom forces water out the top. Weighings indicated that the water removed was 10% of the pore volume as it should be if the pores become full of ice under low pressure.

After freezing, the two halves are cemented together and placed in the solenoid within the pressure vessel. The fluid in the vessel is a coolant kept at a low temperature by pumping in liquid nitrogen. A thermocouple located 2 cm inside the rock next to the midplane is used to record the rock temperature immediately before charge detonation.

2.2 ROCK PROPERTIES

Table 1 lists properties of the Indiana limestone used in our experiments. Our material properties tests were augmented considerably by the work in References 1 through 4 on the same and similar limestone, all from the same general area of the quarry.*

Table 2 lists properties of the Sierra White granite** extracted from the results in Reference 5. Our own measurements on density, porosity, and wave velocities agreed with those listed in Table 2.

2.3 EXPERIMENTS PERFORMED

Table 3 lists the eight experiments performed on the frozen rock, five with Indiana limestone and three with Sierra White granite. For each pore condition, attempts were made to provide two or three identical tests to exhibit the degree of reproducibility (see Appendix A).

*Elliott Stone Co., Inc., 3326 Mitchell Road, P.O. Box 756, Bedford, Indiana 47421.

**Raymond Granite Co., Raymond, California.

Table 1

PROPERTIES OF INDIANA LIMESTONE¹⁻⁴

Density	As received ^a	2.277 grams/cm ³	
	Dry ^b	2.269 grams/cm ³	
	Saturated ^c	2.425 grams/cm ³	
	Grain ^d	2.699 grams/cm ³	
Porosity	Total ^c	15.90%	
	Interconnected ^c	15.54%	
	Occluded ^c	0.36%	
Crush strength	As received ^e	45.8 MPa	
	Dried ^f	53.3 MPa	
P-wave speed	Dry ^g	4.21 mm/ms	
	Saturated ^g	4.35 mm/ms	
S-wave speed	Dry ^g	2.14 mm/ms	
	Saturated	2.09 mm/ms	
Static elastic constants	Bulk modulus, K _S	15 GPa	
	Young's modulus, E _S	22.5 GPa	
	Shear modulus, G _S	9 GPa	
	Poisson's ratio, ν _S	0.25	
Dynamic elastic constants ^h	Dry	Bulk modulus, K	26.5 GPa
		Young's modulus, E	27.8 GPa
		Shear modulus, G	10.4 GPa
		Poisson's ratio, ν	0.33
	Saturated	Bulk modulus, K	31.8 GPa
		Young's modulus, E	28.6 GPa
		Shear modulus, G	10.6 GPa
		Poisson's ratio, ν	0.35
Static failure envelope	Dry	$\sigma_r(s) - \sigma_\theta(s) = 4.17 [\sigma_m(s)]^{0.75}$ MPa	
	Saturated	$\sigma_r(s) - \sigma_\theta(s) = 100$ MPa	
	Crush curve	References 1-3	

Average properties from following numbers of tests

a. 20, b 8, c. 5, d. 5, e. 8, f. 3, g. 10

h. From densities and P- and S-wave measurements

Table 2

PROPERTIES OF SIERRA WHITE GRANITE⁵

Density	Dry	2.638 grams/cm ³			
	Saturated	2.646 grams/cm ³			
	Grain	2.660 grams/cm ³			
Porosity	Total	0.82%			
	Interconnected	0.80%			
	Occluded	0.02%			
Axial stress under uniaxial strain	5	40	125	MPa	
P-wave velocity	5.486	5.934	6.081	mm/μs	
S-wave velocity	3.076	3.398	3.540	mm/μs	
Bulk modulus	Static	18.0	44.1	55.9	GPa
	Dynamic	46.3	52.5	53.7	GPa
Young's modulus	Static	35.8	72.4	79.7	GPa
	Dynamic	63.6	76.8	82.5	GPa
Shear modulus	Static	15.3	29.5	31.5	GPa
	Dynamic	25.0	30.6	33.1	GPa
Poisson's ratio	Static	0.17	0.23	0.26	
	Dynamic	0.27	0.26	0.24	

Table 3
SPHERICAL WAVE EXPERIMENTS PERFORMED WITH
FROZEN ROCK

Rock Type	Pore Condition	Temperature (°C)	Test Number
Indiana limestone	Dry	-8	597
		-8	598 ^a
	Saturated	-8	600
		-16	602 ^a
		-4	605
Sierra White granite	Saturated	-8	590
		-8	591 ^a
		-5	603

^aExperiments selected to illustrate results in Section 3.

The results for Test 590 were suspect in being well outside our experience with Sierra White granite. Consequently, the results are not reported in Appendix A.

Table 4 lists six experiments selected from our past work^{6,7} with spherical waves in Indiana limestone and Sierra White granite at room temperature so that we can compare the waves with those generated in the frozen rocks. The comparisons are made in Section 4.

Table 4
ROOM TEMPERATURE SPHERICAL WAVE RESULTS
USED FOR COMPARISONS^{6,7}

Rock Type	Pore Condition	Test Number
Indiana limestone ^a	Dry	596, 599
	Saturated	601, 604
Sierra White Granite ^b	Dry	564
	Saturated	563

SECTION 3

EXPERIMENTAL RESULTS

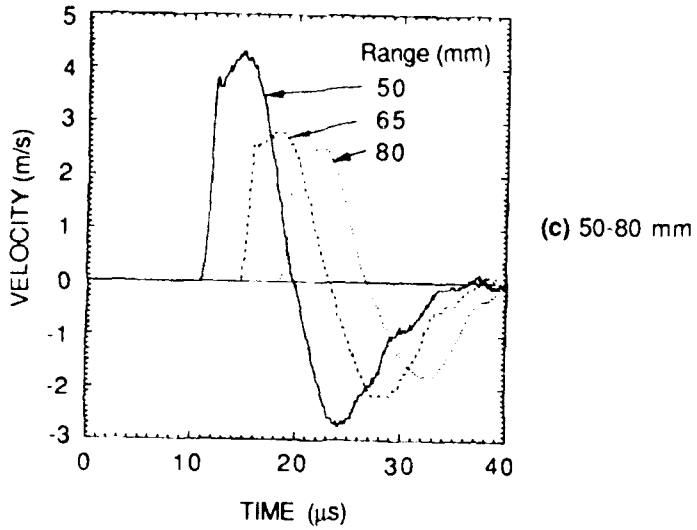
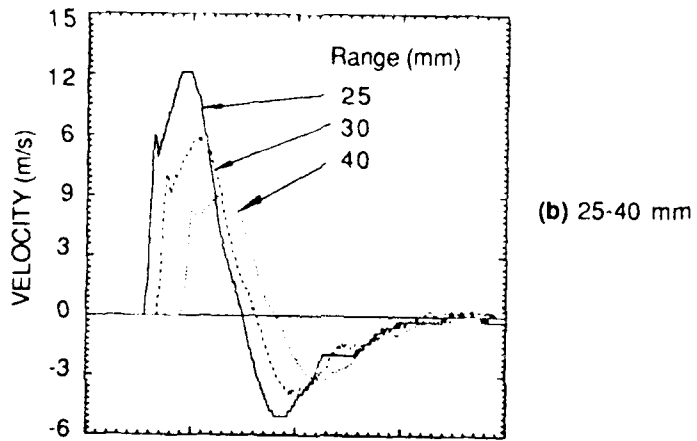
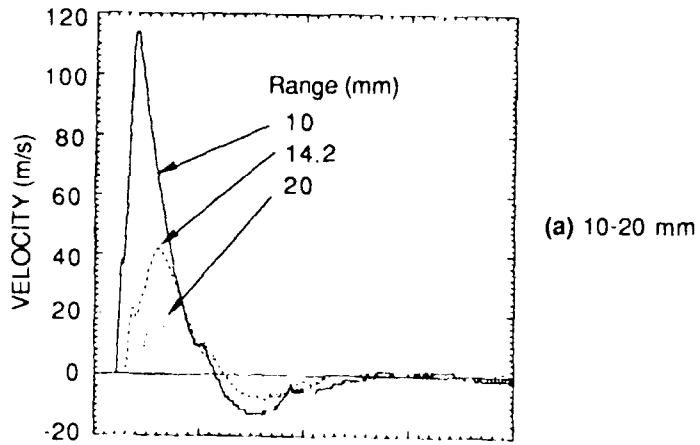
In this section, we present results obtained in frozen rock experiments selected from the complete set listed in Table 3. The frozen/dry and frozen/saturated conditions of Indiana limestone are presented by Tests 598 and 602, and the frozen/saturated condition of Sierra White granite is represented by Test 591. The results for the other experiments listed in Table 3 are shown in Appendix A, where we also show the degree of reproducibility.

3.1 INDIANA LIMESTONE RESULTS

3.1.1 Particle Velocity

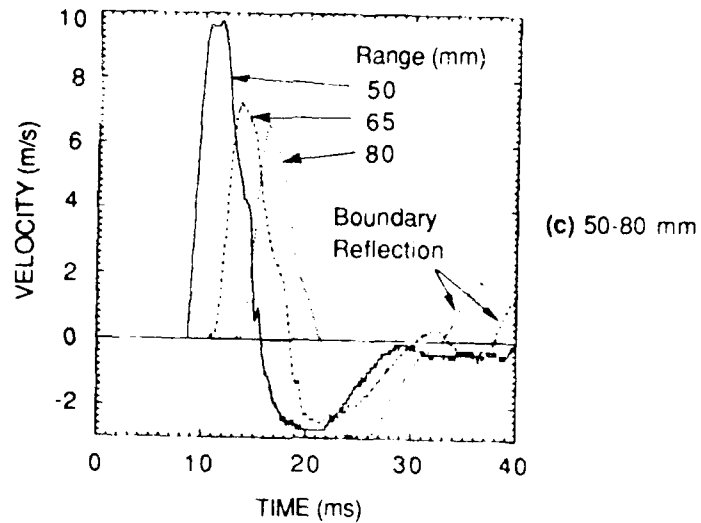
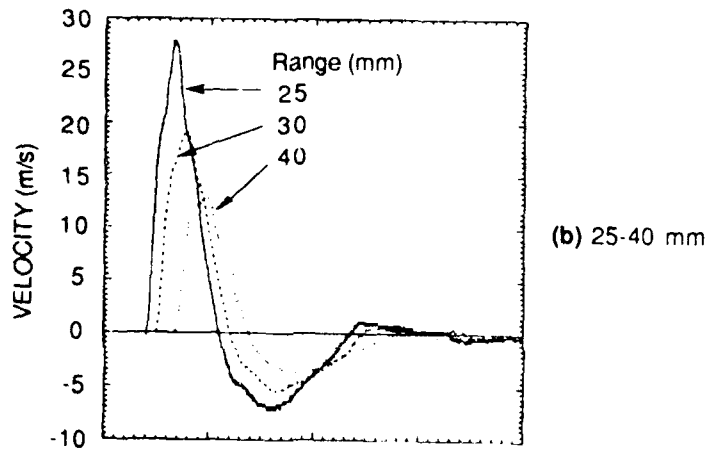
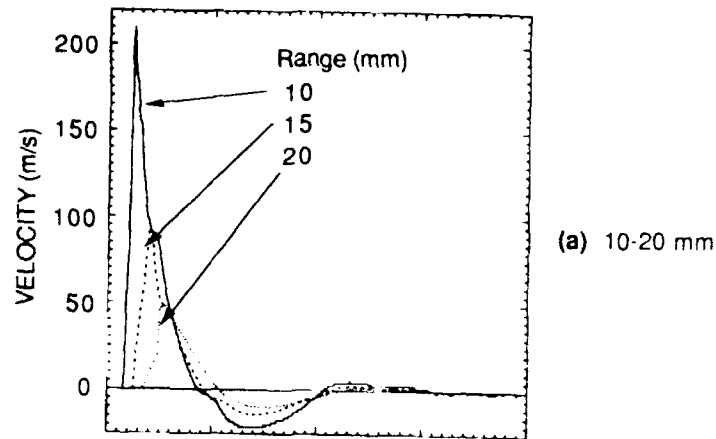
Figure 2 shows the nine particle velocity records obtained from Test 598 in which the limestone was in a frozen/dry condition. Arrival times of the wave front at the particle velocity gage ranges determine a constant velocity of $4.4 \text{ mm}/\mu\text{s}$. A distinctive feature of the wave shape is the initial rapid rise that corresponds to an elastic precursor. Preliminary elastic analysis indicates that, at the shorter ranges [Figure 2(a)], the precursor wave magnitude is governed by the onset of pore crushing. At the remaining larger ranges, the entire wave is elastic. Following the precursor, the particle velocity increases at a slower rate to a peak value. After the peak is reached, the velocity decays steadily to form an outwardly directed pulse of $9\text{-}\mu\text{s}$ duration. The wave then exhibits an inwardly directed phase of substantial magnitude for an addition $16 \mu\text{s}$.

Figure 3 shows the nine particle velocity records obtained from Test 602 in which the limestone was in a frozen/saturated condition. Arrival times at the gage ranges give a constant wave velocity of $5.6 \text{ mm}/\mu\text{s}$, which is much faster than the wave velocity in frozen/dry limestone ($4.4 \text{ mm}/\mu\text{s}$). An elastic precursor exists, but it is less pronounced than the precursor in frozen/dry limestone. The overall pulse shapes are similar to those in Figure 2, but the maximum velocities are about twice the frozen/dry values, the duration of outward motion is shorter ($7 \mu\text{s}$ compared with $9 \mu\text{s}$) as is the rebound duration ($13 \mu\text{s}$ compared with $16 \mu\text{s}$), and the magnitudes of the rebound velocities are comparable.



CM-1676-21

Figure 2. Particle velocity histories measured at nine ranges in dry/frozen Indiana limestone, Test 598.



CM-1676-22

Figure 3. Particle velocity histories measured at nine ranges in saturated/frozen Indiana limestone, Test 602.

3.1.2 Displacement

Figure 4 shows the nine displacement histories obtained from Test 598 in which the limestone was in a frozen/dry condition. The curves were obtained by temporal integration of the particle velocity records in Figure 2. At each range, the displacement achieves a final value after reaching its maximum value, which demonstrates that the explosive cavity has undergone permanent enlargement.

Figure 5 shows the corresponding displacement histories for frozen/saturated conditions. The maximum displacements are larger by a percentage depending on the range, as are the final displacements.

3.1.3 Reduced Velocity Potential (RVP)

Figure 6 shows the RVPs obtained from Test 598 for frozen/dry limestone. The function is fairly constant beyond a range of 20 mm (4 charge radii), so this range is an estimate for the elastic radius.

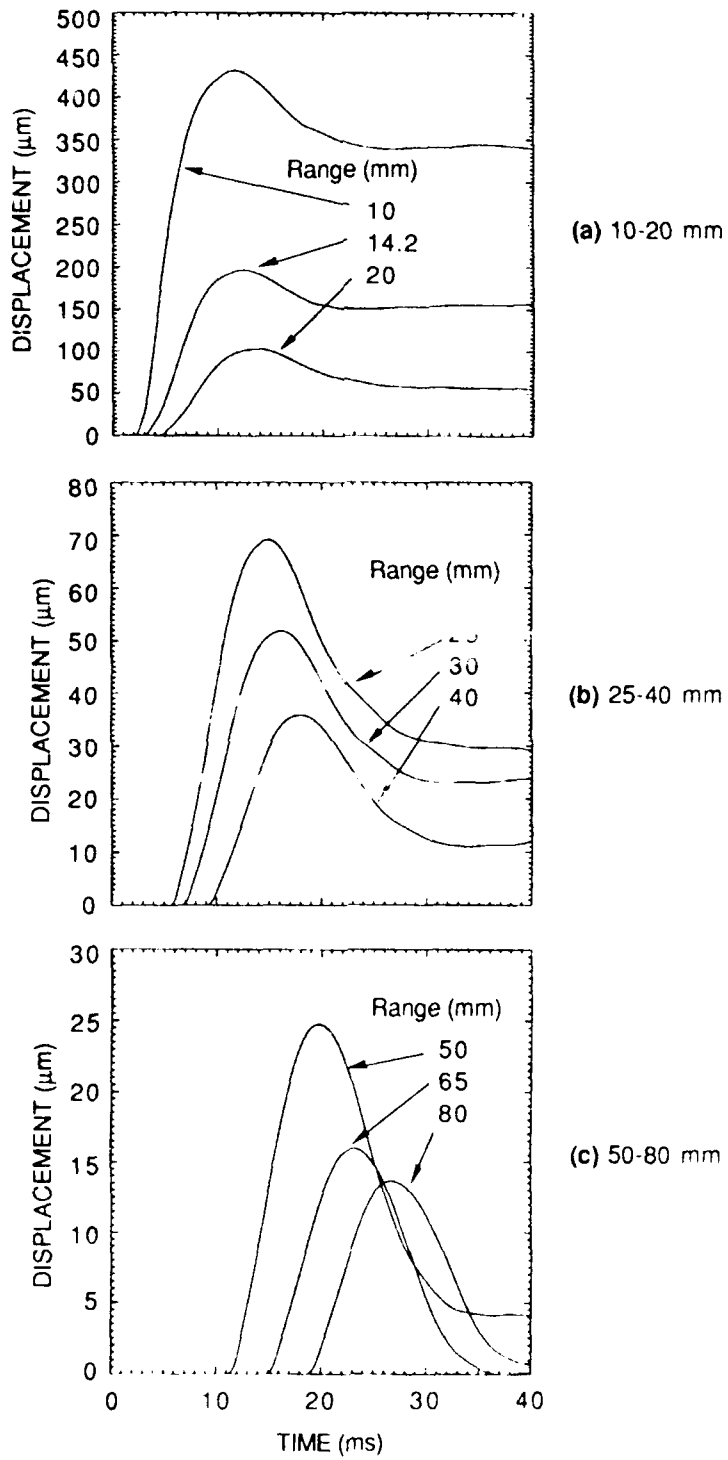
Figure 7 shows the RVPs obtained from Test 602 for frozen/saturated limestone. The function is fairly constant beyond a range of 25 mm (5 charge radii), so this range is an estimate for the elastic radius.

3.1.4 Reduced Displacement Potential (RDP)

Figures 8 and 9 show the RDPs obtained from Tests 598 and 602 for frozen/dry and frozen/saturated limestone, respectively. In Figure 8, we see that the function is fairly constant beyond a range of 20 mm. In Figure 9, the results for the outer three ranges are not accurate enough to allow conclusions to be drawn. However, by smoothing the final displacements by means of a least squares fit to $\xi_{\infty} = \psi_{\infty}/r^2$ ($r \geq 20$ mm), we obtain $\psi_{\infty} \approx 0.021$ and $0.031 \text{ mm}^3 \times 10^{-3}$ for the final asymptotic values of the dry and saturated RDP, respectively.

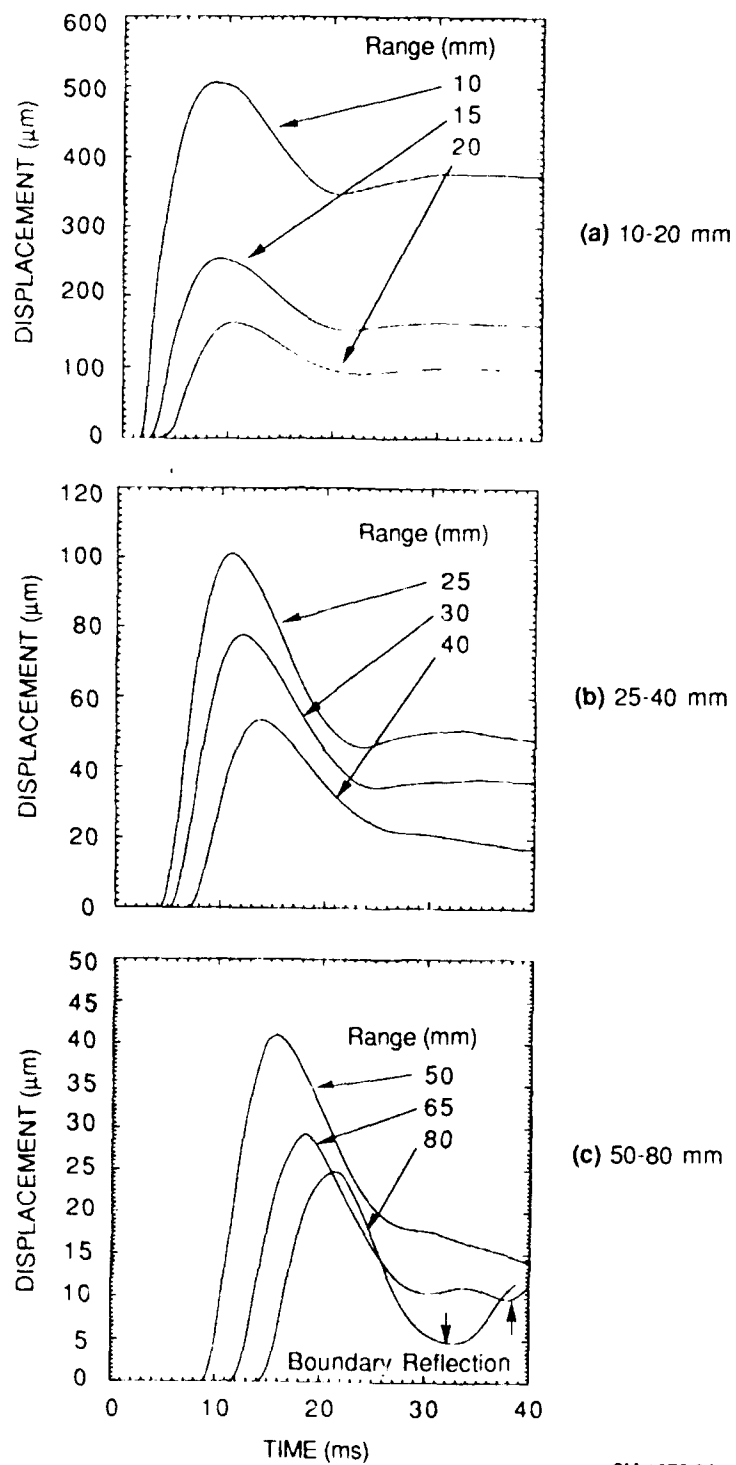
3.1.5 Additional Results

Various spectral distributions, attenuation plots, wave velocities, and radiated kinetic energies are provided in Section 4 where we compare the results for frozen/dry, frozen/saturated, and room temperature dry and saturated limestone.



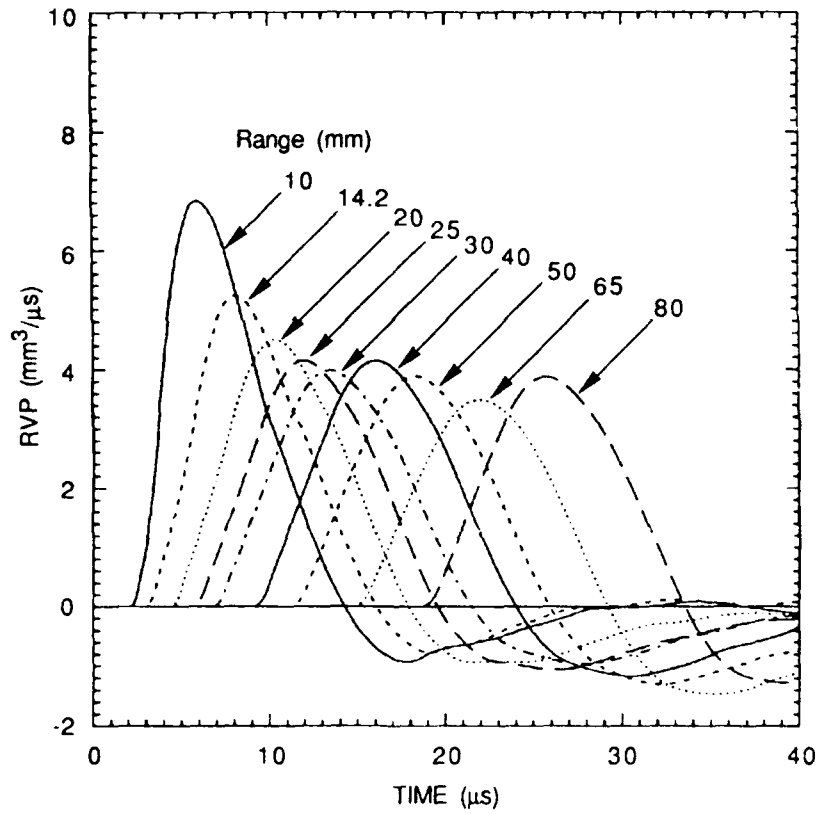
CM-1676-23

Figure 4. Displacement histories measured at nine ranges in dry/frozen Indiana limestone, Test 598.



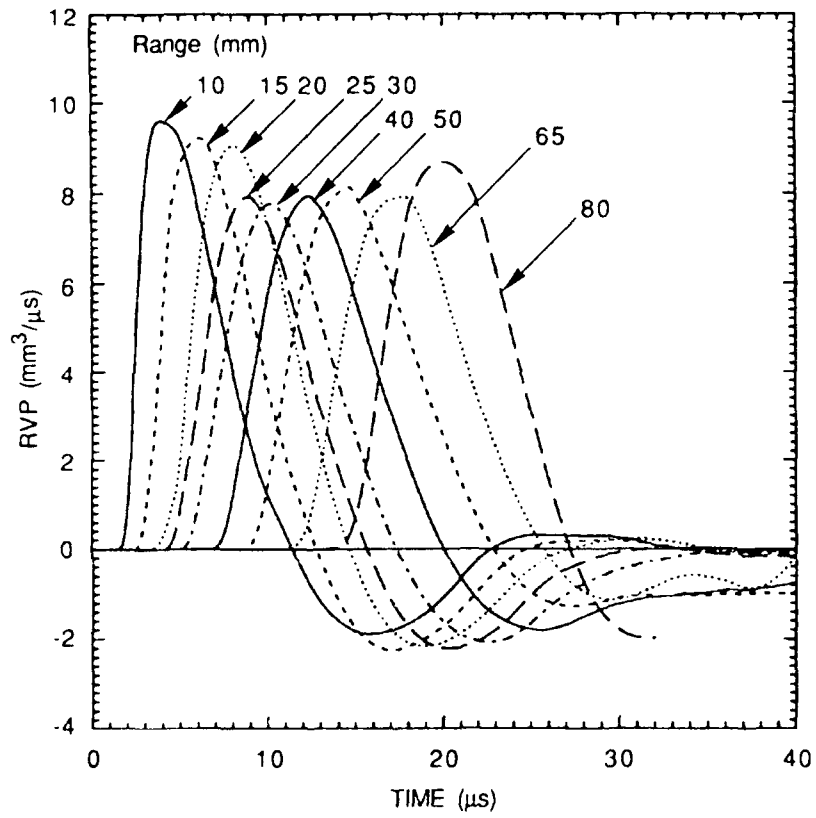
CM-1676 24

Figure 5. Displacement histories measured at nine ranges in saturated/frozen Indiana limestone, Test 602.



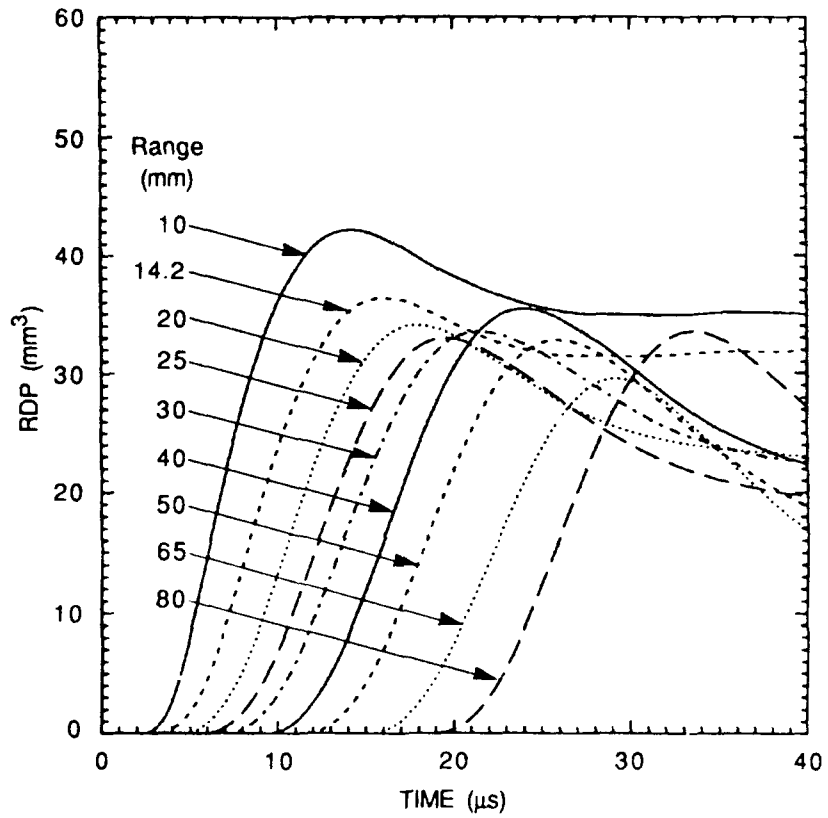
CM-1676-25

Figure 6. Reduced velocity potential histories measured in dry/frozen Indiana limestone, Test 598.



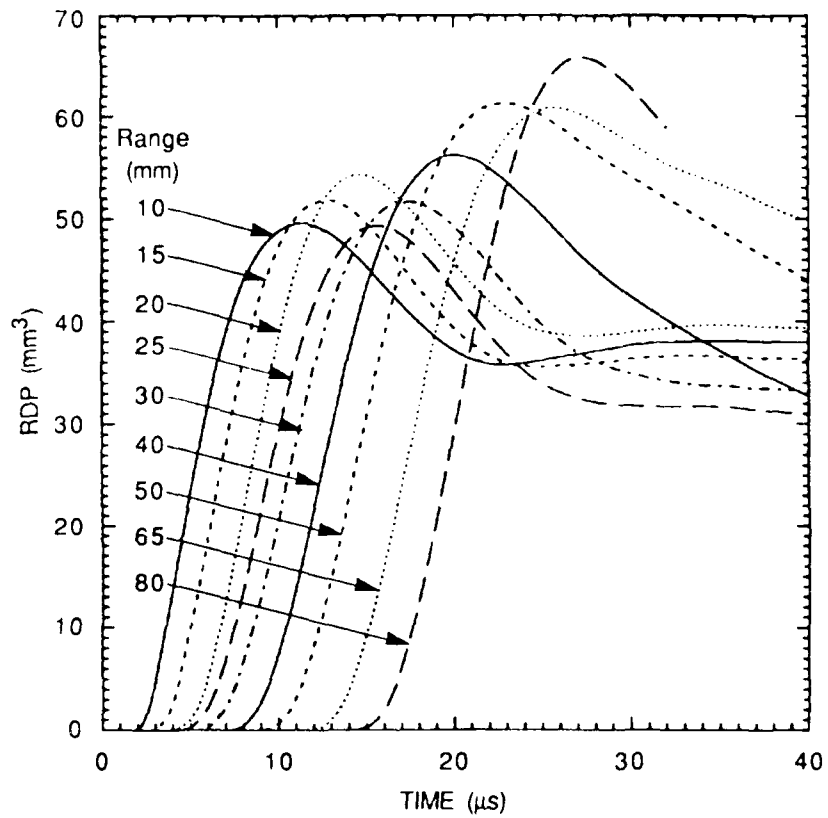
CM-1676-26

Figure 7. Reduced velocity potentials measured in saturated/frozen Indiana limestone, Test 602.



CM-1676-27

Figure 8. Reduced displacement potentials measured in dry/frozen Indiana limestone, Test 598.



CM-1676-28

Figure 9. Reduced displacement potentials measured in saturated/frozen Indiana limestone, Test 602.

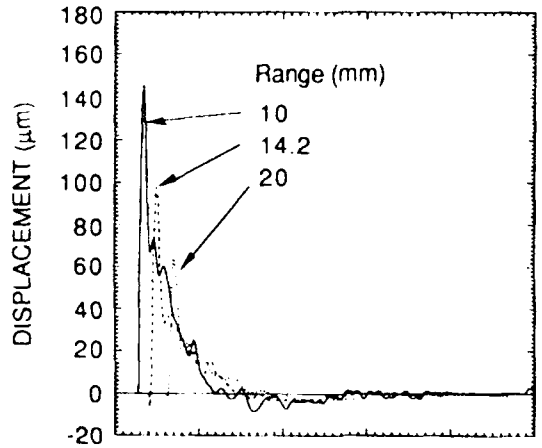
3.2 SIERRA WHITE GRANITE RESULTS

As shown in Table 3, all experiments on granite were in the frozen/saturated condition. Because the particle velocity records, as represented by the results in Figure 10 for Test 591, are almost identical to past records from tests with dry and saturated Sierra White granite performed at room temperature, it seems reasonable to assume that frozen/dry conditions would not give different records.

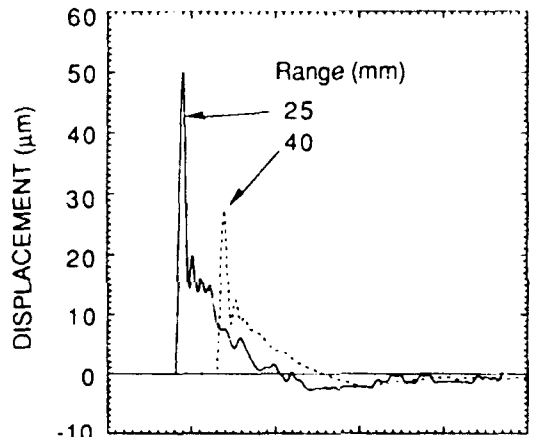
The main features of the particle velocity records consist of a sharp rise to the peak velocity (no precursor at the stress levels of these experiments) followed by a smooth decay to form an outwardly directed velocity pulse of 6- μ s duration and a rebound of comparable duration. The corresponding displacements are shown in Figure 11. Permanent displacements occur, which indicates that the explosive cavity was permanently enlarged. Figure 12 shows the RVP function with a behavior consistent with the development of elastic wave propagation within a short distance of the charge. Figure 13 shows the RDP function. Data smoothing or analytic fitting is required for such short pulses (Figure 10) to overcome inaccuracies in the raw data and provide a generic RDP.

Figure 14 shows the spectral distribution of the particle velocity measured at a range of 25 mm (5 charge radii). The amplitudes form a plateau at about 60 (m/s)/MHz up to 50 kHz, above which the spectral amplitudes decrease with frequency, f , as $f^{-0.69}$ up to 1 MHz. Figure 15 shows the corresponding spectral distribution for the displacement, with the lower frequencies having a plateau at 110 μ m/MHz to 50 kHz and a decrease as $f^{-0.84}$ up to 1 MHz. If our experiments represent a scaled yield of 8 kt TNT equivalent, the scale factor is 2550 and the corner frequency of 50 kHz becomes 20 Hz.

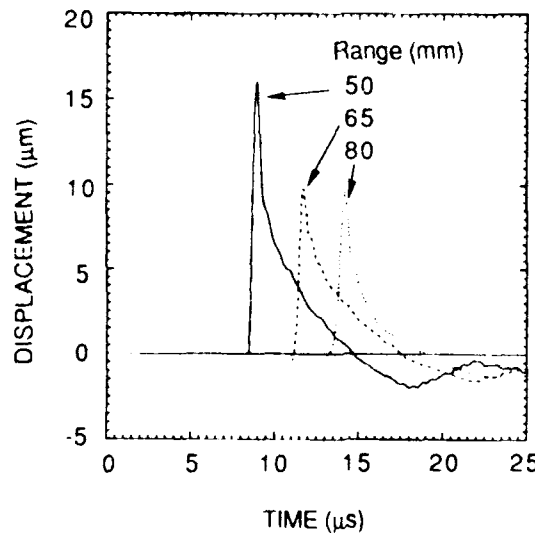
Figures 16 and 17 show the corresponding spectra for the RVP and RDP provided by the particle velocity data at a range of 25 mm. The amplitude distributions are similar to those of the particle velocity and displacement spectra shown in Figures 16 and 17. The amplitudes for the higher frequencies (>50 kHz) decay as $f^{-1.53}$ and $f^{-1.04}$ in the RVP and RDP spectra, respectively.



(a) 10-20 mm



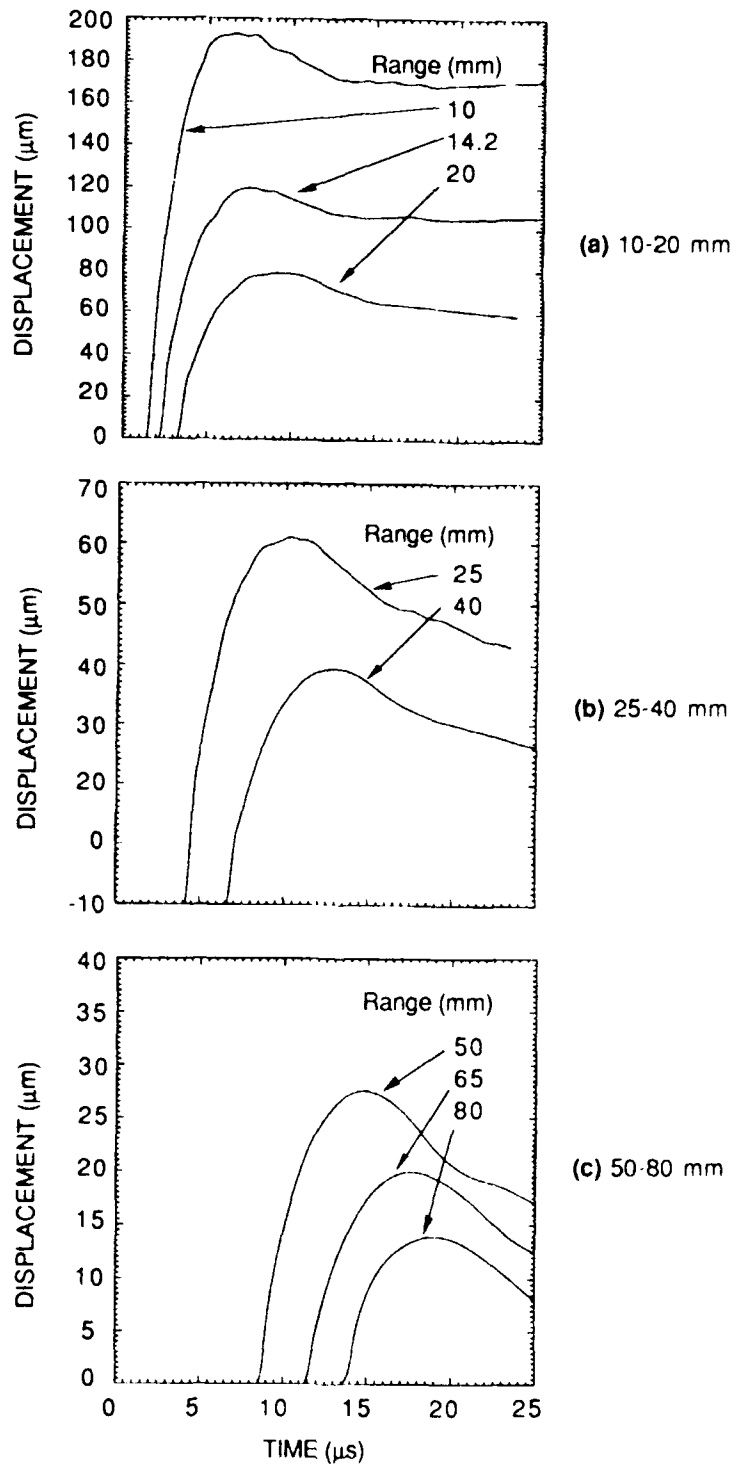
(b) 25-40 mm



(c) 50-80 mm

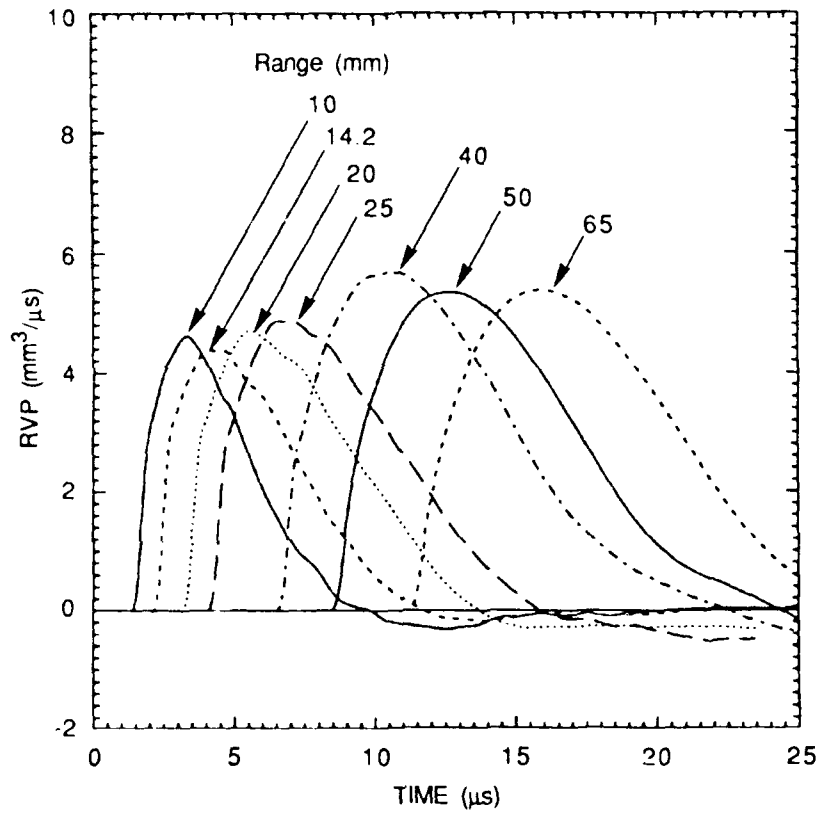
CM-1676-38

Figure 10. Particle velocity histories measured at eight ranges in saturated/frozen Sierra White granite, Test 591.



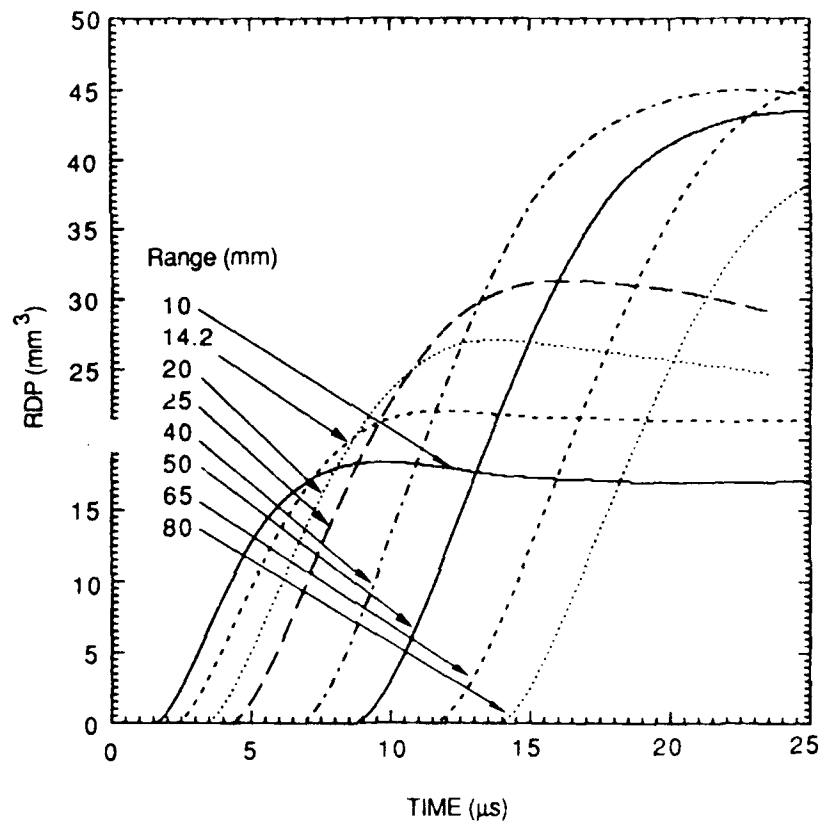
CM-1676 39

Figure 11. Displacement histories measured at eight ranges in saturated/frozen Sierra White granite, Test 591.



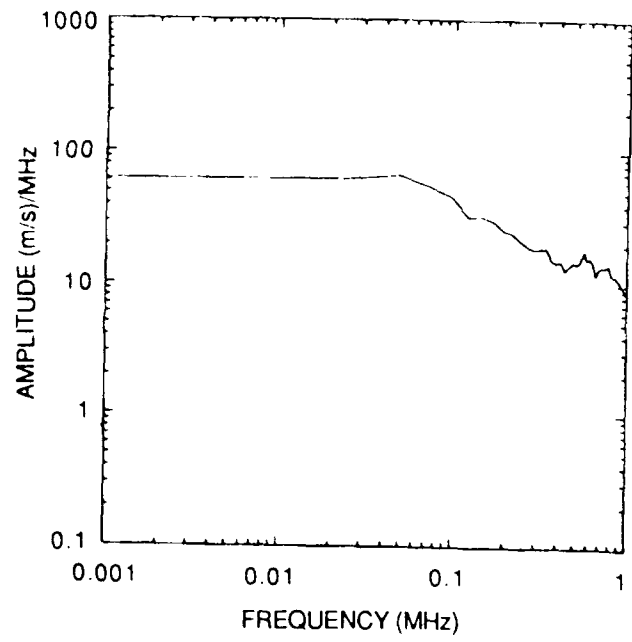
CM-1676-40

Figure 12. Reduced velocity potential histories measured in saturated/frozen Sierra White granite, Test 591.



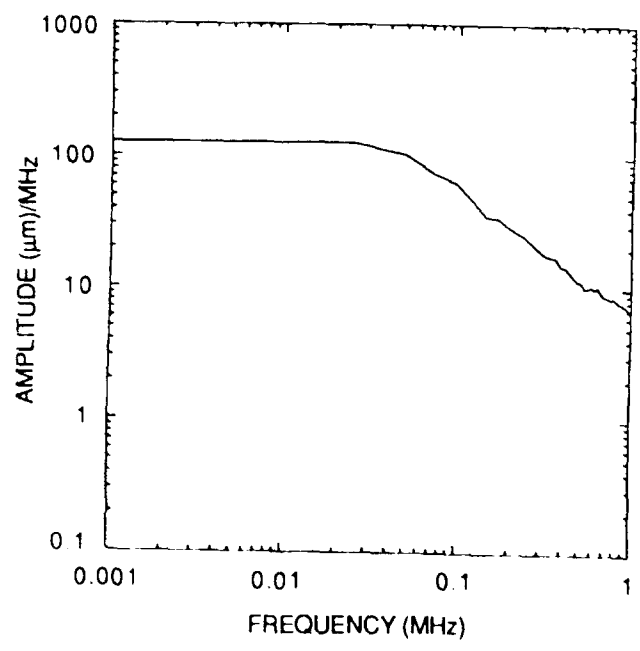
CM 1676-44

Figure 13. Reduced displacement histories measured in saturated/frozen Sierra White granite, Test 591.



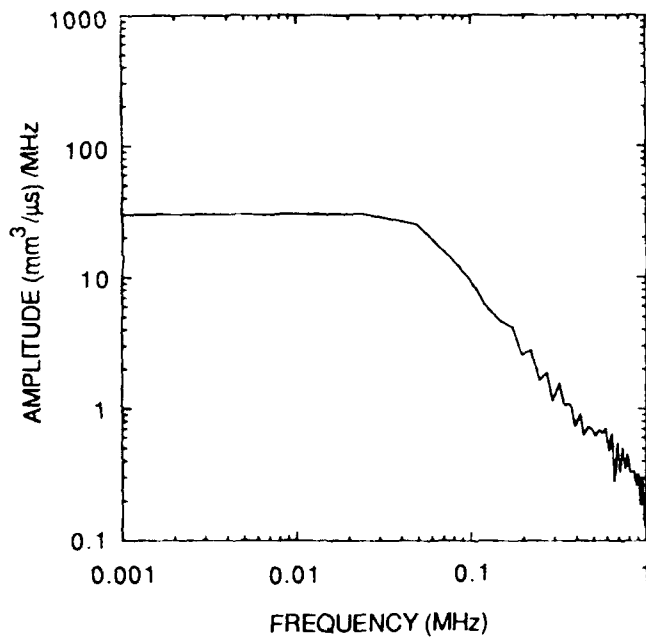
CAM-1676-49

Figure 14. Velocity spectra measured at 25-mm range in saturated/frozen Sierra White granite, Test 591.



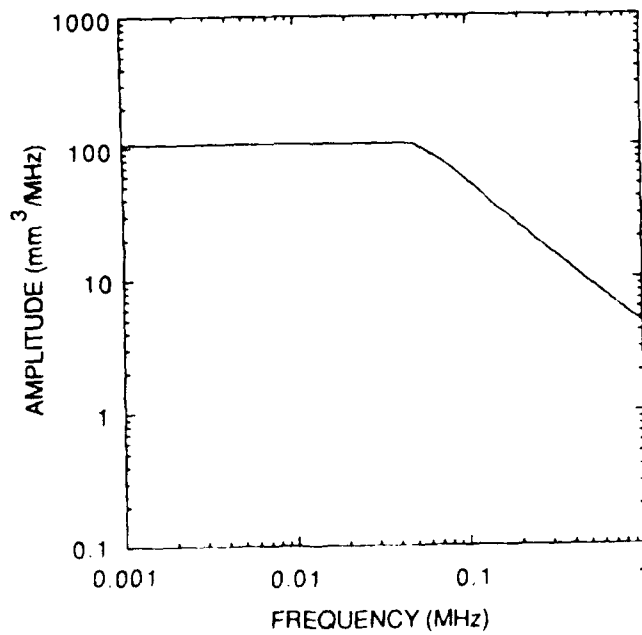
CM-1676-50

Figure 15. Displacement spectra ($\xi - \xi_{\infty}$) measured at 25-mm range in saturated/frozen Sierra White granite, Test 591.



CM-1676-51

Figure 16. Reduced velocity potential spectra measured at 25-mm range in saturated/frozen Sierra White granite, Test 591.



CM-1676-52

Figure 17. Reduced displacement potential spectra ($\psi - \psi_{\infty}$) measured at 25-mm range in saturated/frozen Sierra White granite.

SECTION 4

COMPARISON OF EXPERIMENTAL RESULTS

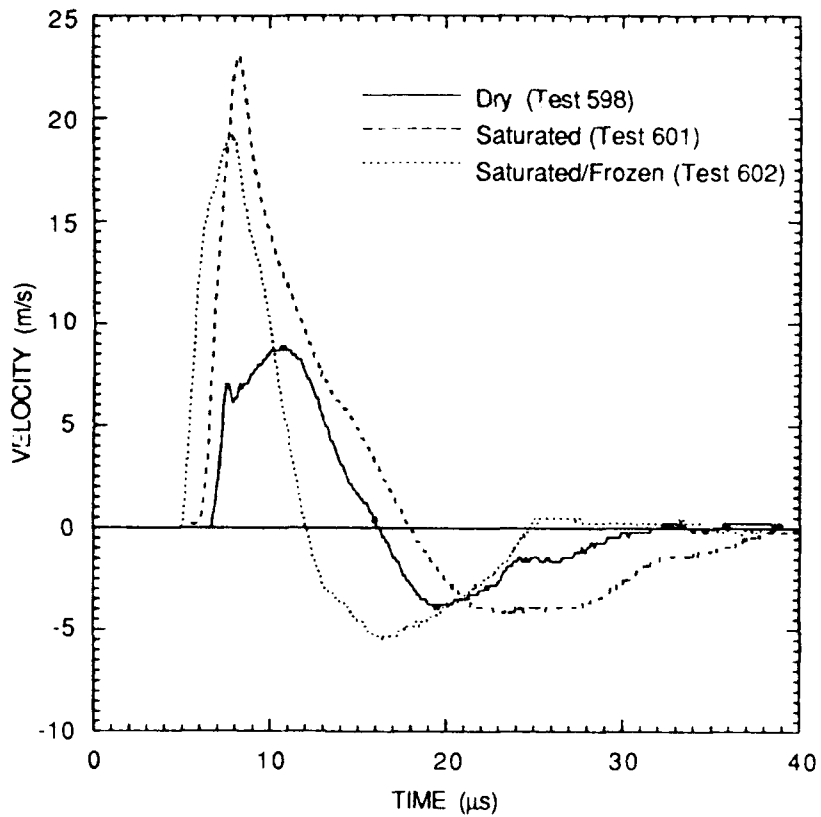
We compare the results of the frozen rock experiments with those available from room temperature experiments on rock having the same basic properties as listed in Tables 1 and 2 in Section 2. Freezing of the rock made no significant difference to the wave profiles measured in Sierra White granite nor to the wave profiles in dry Indiana limestone. Our comparisons are consequently reduced to a comparison of the results of frozen/saturated Indiana limestone with those from room temperature saturated conditions performed under Contract DNA 001-90-C-0131 (Test 601, Reference 6). The results from frozen/dry conditions (same as room temperature results) are included to show the effect of saturation.

The results presented consist of particle velocity, displacement, RVP, RDP, and spectra of these quantities all at the same range (30 mm). In addition, we compare wave speeds, attenuation plots of maximum velocities and displacements, and the radiated kinetic energy.

4.1 INDIANA LIMESTONE

4.1.1 Particle Velocity

Figure 18 shows the particle velocity records for the three conditions at a range of 30 mm (6 charge radii), which is beyond the elastic radius in all cases. Freezing the saturated limestone had the effect of increasing the wave speed, lowering the maximum velocity, and shortening the outward and inward phases of the pulse when compared to dry and saturated/room temperature conditions. During the initial velocity rise, a precursor wave is visible in Test 602 but not in the repeat Tests 600 and 605 (see Figure A3 in Appendix A where we discuss reproducibility). The change in pulse shape is consistent with the ice providing higher moduli and strength, and reducing the fluidization around the explosive charge that occurs with water-filled pores. In other words, the trend is toward an elastic behavior throughout the material; in fact, the pulse tends to resemble the pulses generated in Sierra White granite.



CM-1676-29

Figure 18. Comparison of velocity histories at 30-mm range in Indiana limestone (16% porosity) for three different pore conditions.

4.1.2 Displacement

Figure 19 shows the displacement histories obtained from the velocity pulses of Figure 18. With time measured from time of arrival at the 30-mm range, the displacements lie between those of the dry and saturated conditions. Because the pulse is shorter, the final displacement plateau is reached sooner.

4.1.3 RVP and RDP

Figures 20 and 21 compare the RVP and RDP functions at a range of 30 mm, respectively. The magnitude of the RVP is not affected by freezing the pore water, but the phase durations are much shorter, as expected by the form of the particle velocity records in Figure 18. The RDP functions bear a relationship to each other that is similar to the displacement histories in Figure 19.

4.1.4 Spectra

Figure 22 shows the spectra of the particle velocities measured at a range of 30 mm. Freezing lowered the low frequency amplitudes by about a factor of 2 and raised the corner frequency from 30 to 50 kHz. The higher frequency contents are similar, with amplitudes decaying as f^{-2} .

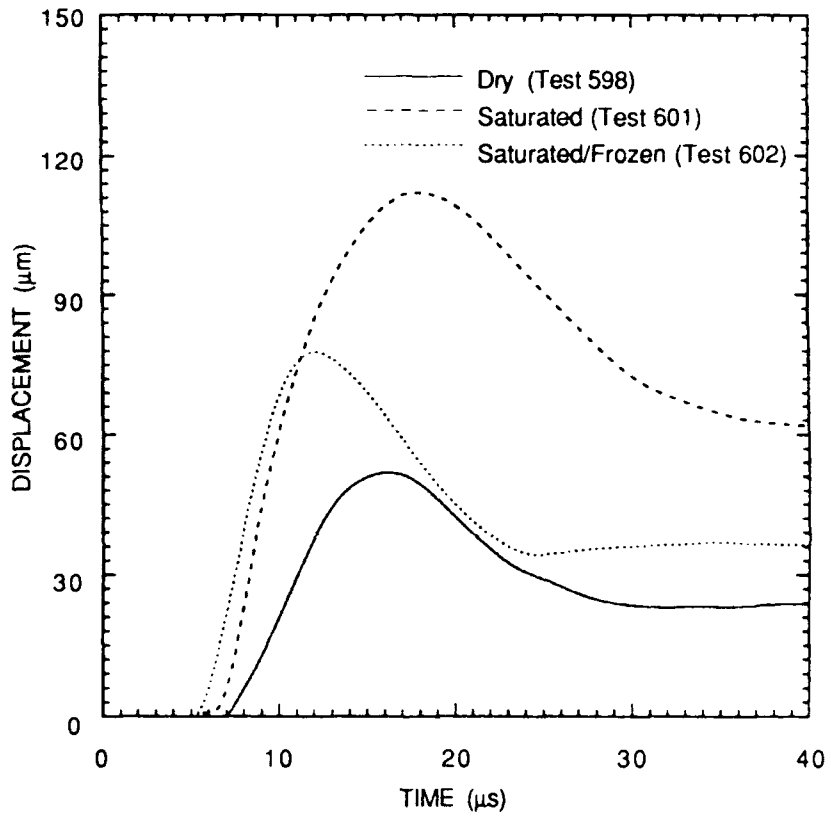
Figure 23 shows the corresponding spectra of the displacements ($\xi - \xi_{\infty}$). Freezing lowered the low frequency amplitudes by about a factor of 2 and raised the corner frequency from 30 to 50 kHz, as in the particle velocity spectra. Freezing lowered the high frequency content generally, but the decay of both is almost inversely proportional to the frequency (f^{-1}).

Figure 24 for the RVP spectra is similar to Figure 22 for the particle velocity spectra so the observation made about Figure 22 apply.

Figure 25 for the RDP spectra is similar to Figure 23 for the displacement spectra so again the observations made about Figure 23 apply.

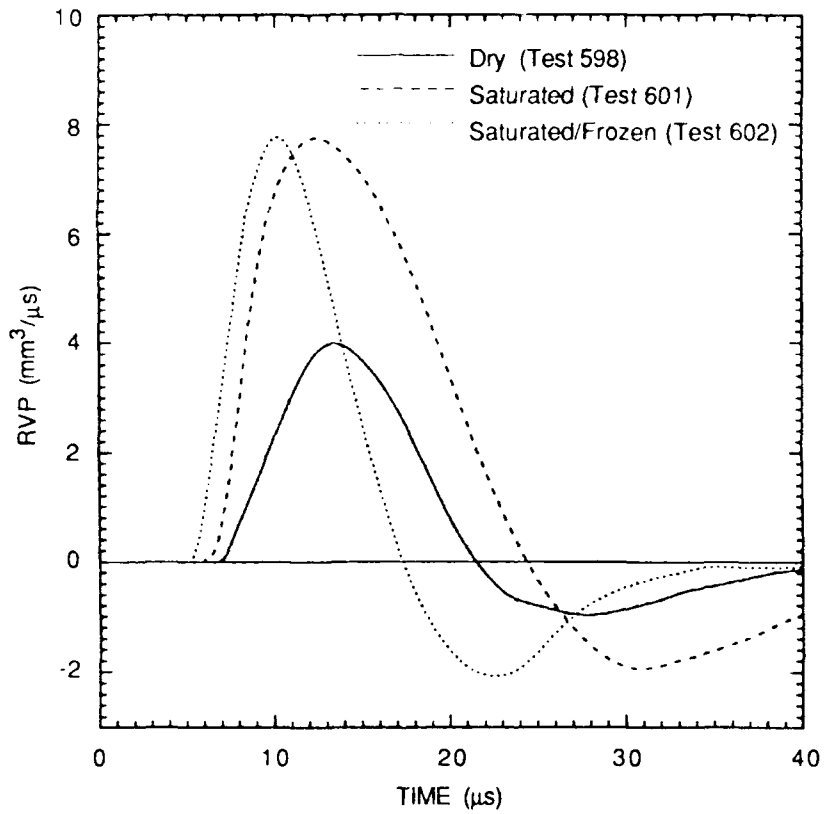
4.1.5 Other Comparisons

Figure 26 shows plots of the times of arrival at the various gage ranges. The plots are linear and the inverse slopes give the wave velocities. Freezing saturated limestone increases the wave speed considerably from 4.7 mm/ μ s to 5.6 mm/ μ s, which is about the same as the wave speed in Sierra White granite.



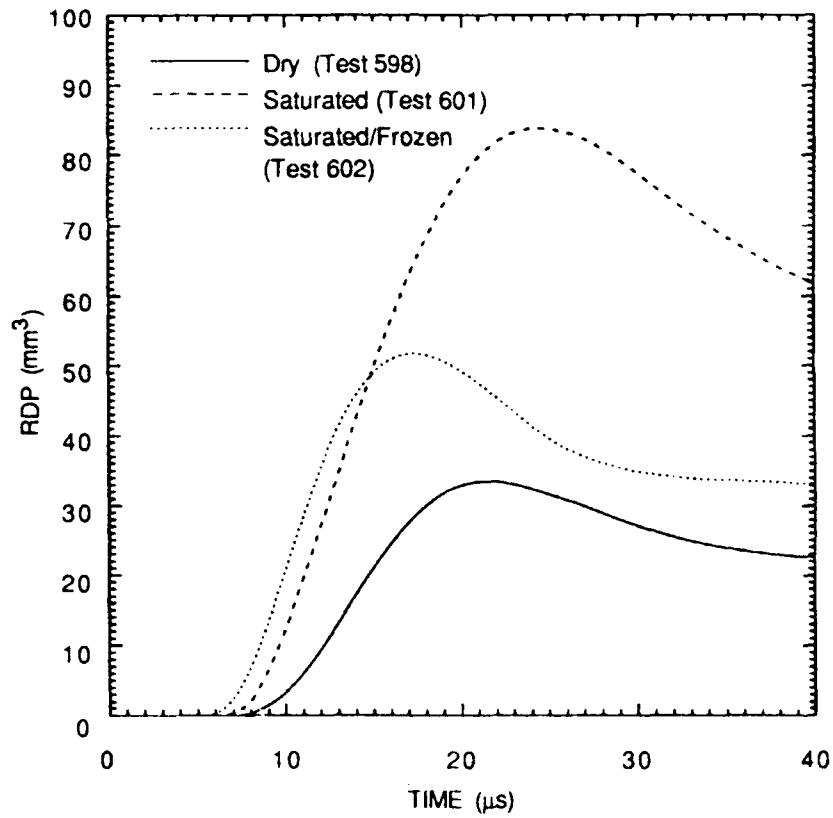
CM-1676-30

Figure 19. Comparison of displacement histories at 30-mm range in Indiana limestone (16% porosity) for three different pore conditions.



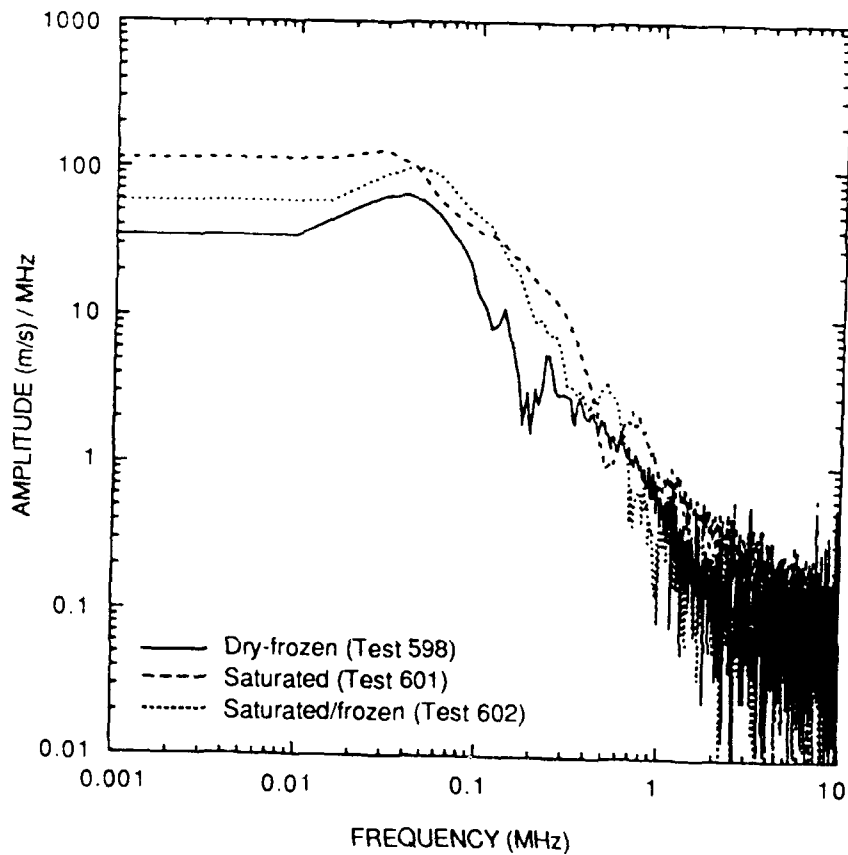
CM-1676-31

Figure 20. Comparison of reduced velocity potential histories at 30-mm range in Indiana limestone (16% porosity) for three different pore conditions.



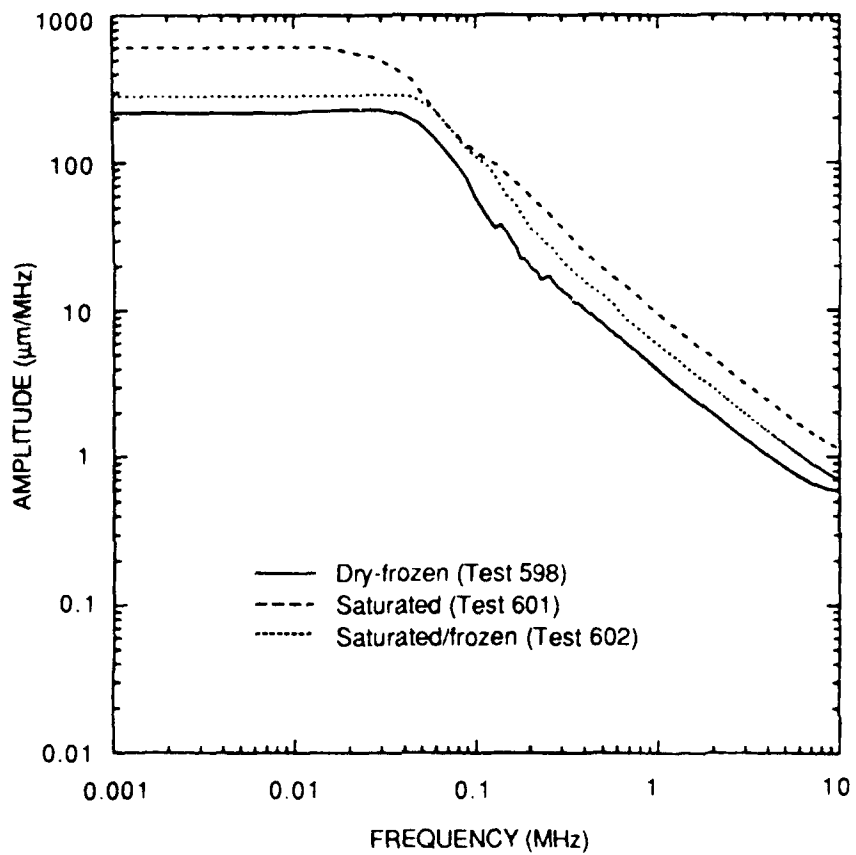
CM-1676-32

Figure 21. Comparison of reduced displacement potential histories at 30-mm range in Indiana limestone (16% porosity) with three different pore conditions.



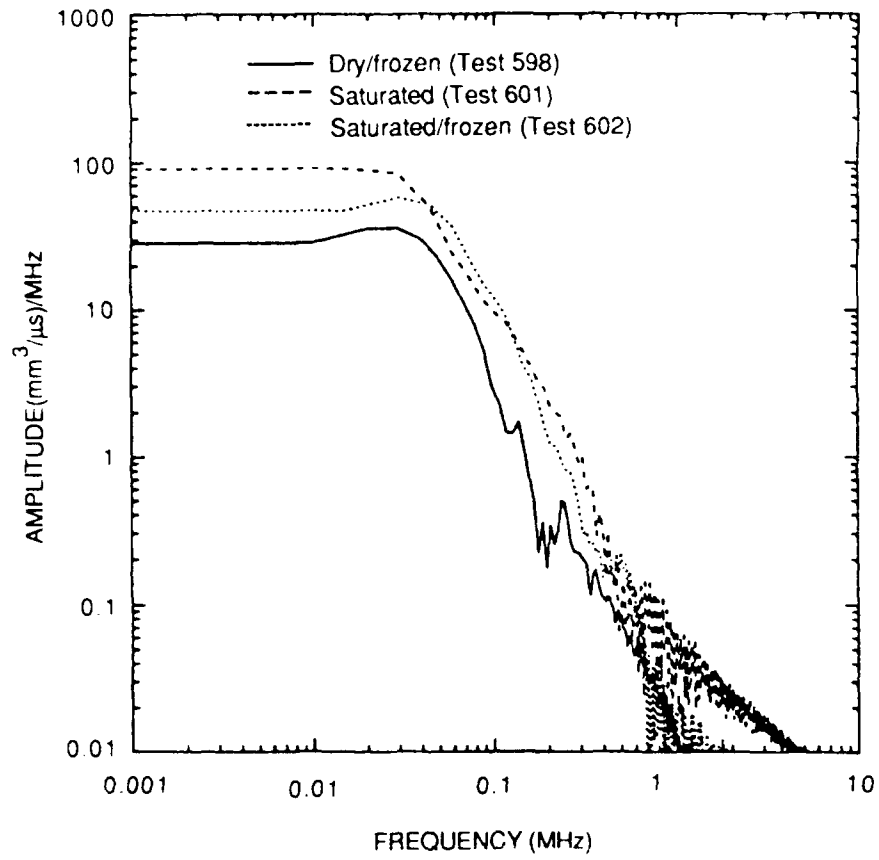
CM-1676-33

Figure 22. Comparison of velocity spectra at the 30-mm range in Indiana limestone (16% porosity) with three different pore conditions.



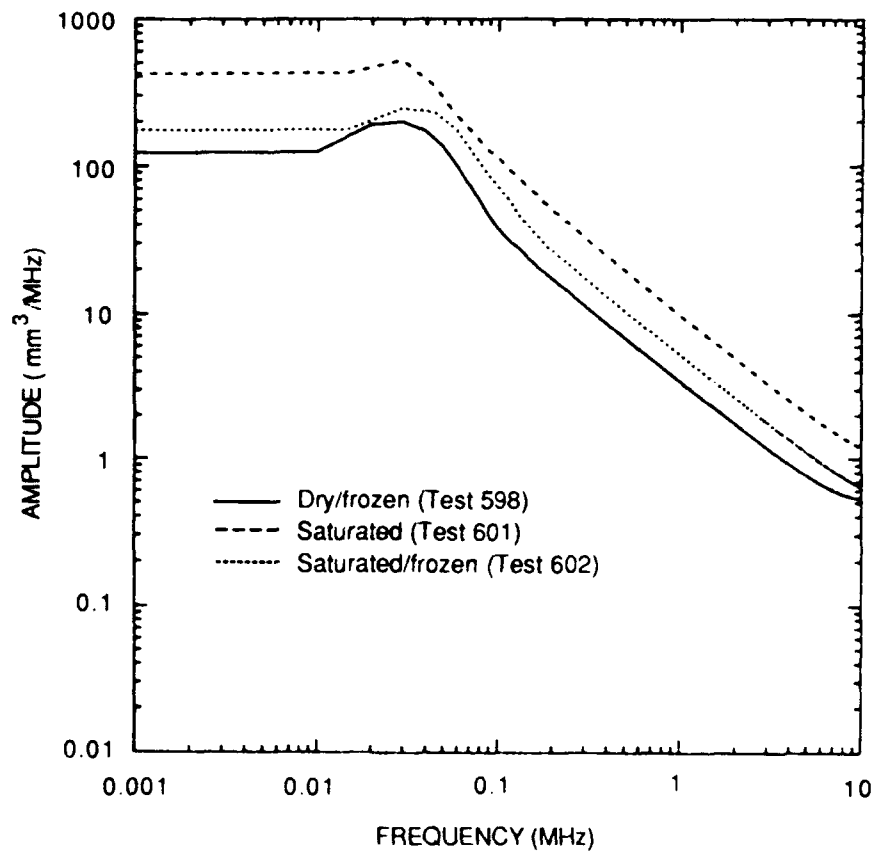
CM-1676-34

Figure 23. Comparison of displacement spectra at the 30-mm range in Indiana limestone (16% porosity) with three different pore conditions.



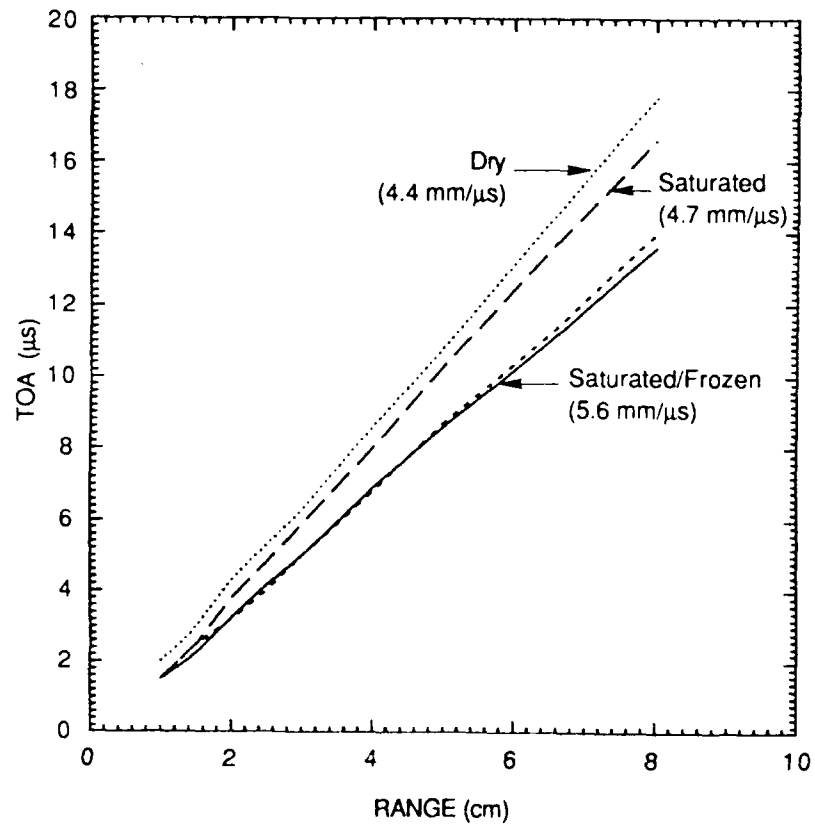
CM-1676-35

Figure 24. Comparison of reduced velocity potential spectra at 30-mm range in Indiana limestone (16% porosity) with three different pore conditions.



CM-1676-36

Figure 25. Comparison of reduced displacement potential spectra at 30-mm range in Indiana limestone (16% porosity) with three different pore conditions.



CM-1676-37

Figure 26. Wave front histories measured in Indiana limestone (16% porosity) for three different pore conditions.

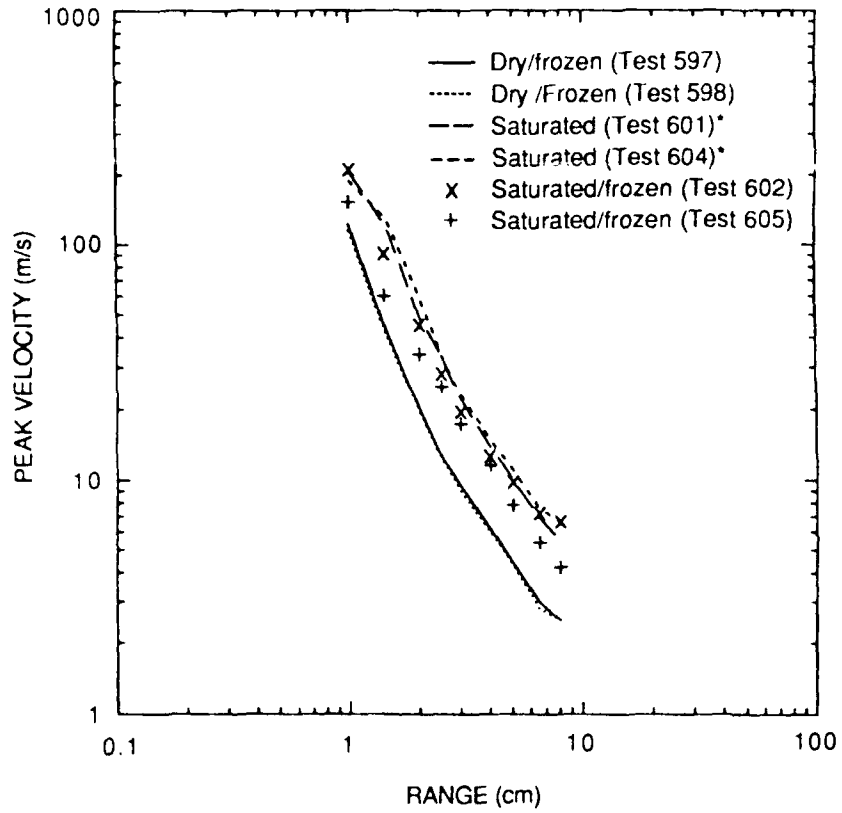
Figure 27 shows the attenuation of the maximum particle velocity with range. Freezing saturated limestone results in lower velocities but similar attenuation curves. Beyond about 20 mm, the attenuation for all cases is in accordance with spherical elastic wave propagation. The maximum values plotted in Figure 27 are listed in Table 5.

Figure 28 shows the attenuation of the maximum displacement with range. Freezing saturated limestone results in lower displacements but similar attenuation curves. The maximum values plotted in Figure 28 are listed in Table 6.

Table 7 lists the radiated kinetic energies in Indiana limestone calculated at four ranges from the particle velocity records. The energies in the saturated and frozen/saturated limestones are similar, being 131J and 138J, respectively. In Sierra White granite, the radiated kinetic energy is about 170J.

4.2 SIERRA WHITE GRANITE

By comparing the particle velocities and displacements in Figures 10 and 11 with the room temperature results from Tests 564 and 563 listed in Table 4, we concluded that freezing Sierra White granite had no effect on the wave propagation characteristics. As an illustration, we see that in Figures 29 and 30, showing the velocity and displacement attenuation plots, the frozen/saturated granite results fall within the scatter of the room temperature results (from Reference 7). The maximum values plotted in Figures 29 and 30 are listed in Tables 8 and 9, respectively.



*Data from Ref. 6

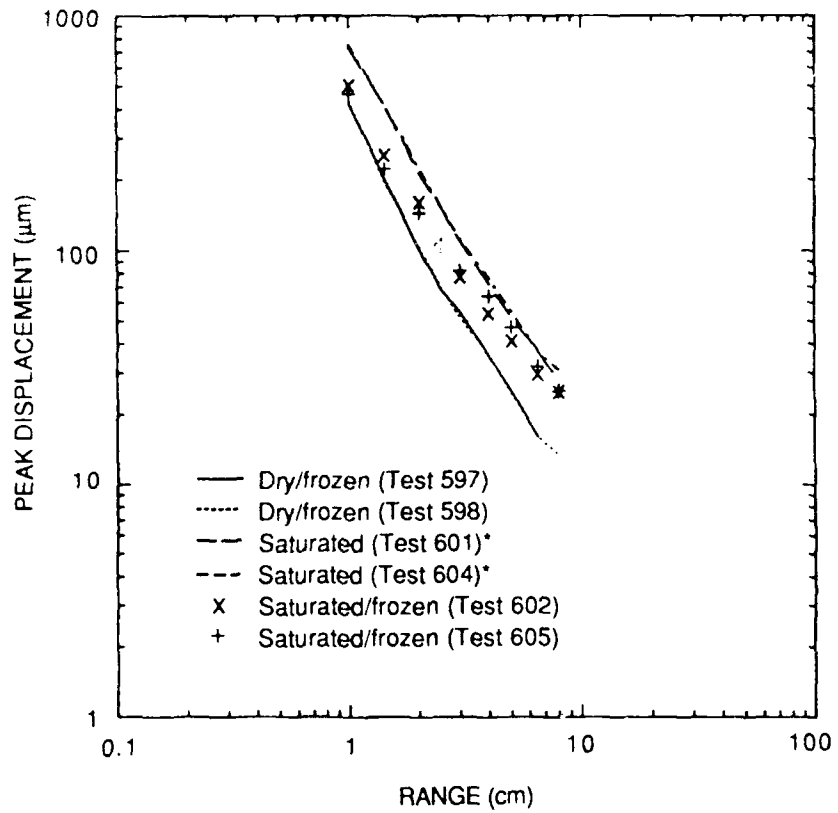
CM-1676-41

Figure 27. Attenuation of peak particle velocity in dry/frozen, saturated, and saturated/frozen Indiana limestone.

Table 5
MAXIMUM PARTICLE VELOCITIES IN
INDIANA LIMESTONE (m/s)

Range (mm)	Frozen Dry		R.T. Dry		Frozen Saturated			R.T. Saturated	
	597 ^a	598	596	599	600	602	605	601	604
10	122	114	120	118	169	210	152	188	207
14.2	44	42	45	44	58	-	60	127	119
15	-	-	-	-	-	91	-	-	-
20	20	19.5	22	18	24	45	34	60	49
25	12.4	12.1	12	11	16	28	20.8	33	33
30	9.4	8.9	9	8.5	11.6	19.4	17.3	23	22
40	6.2	6.0	5.6	-	8.8	12.6	11.6	15	14
50	4.4	4.3	4.3	4	6.8	9.8	7.8	11	10
65	3.0	2.8	3	2.7	4.8	7.2	5.4	7.6	6.9
80	2.5	2.5	2.4	2.2	4.2	6.6	4.2	6.6	5.5

^aTest numbers.



* Data from Ref. 6

CM-1676-42

Figure 28. Attenuation of peak displacement measured in dry/frozen, saturated, and saturated/frozen Indiana limestone.

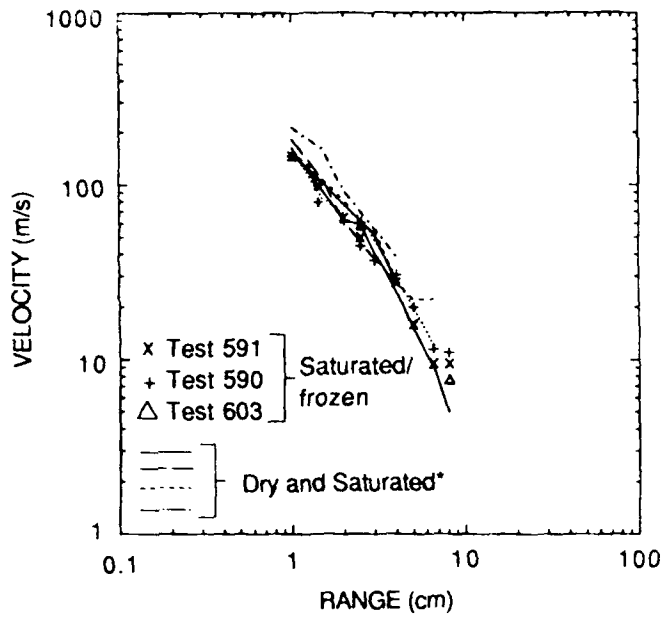
Table 6
**MAXIMUM DISPLACEMENTS IN
 INDIANA LIMESTONE (μm)**

Range (mm)	Frozen Dry		R.T. Dry		Frozen Saturated			R.T. Saturated	
	597 ^a	598	596	599	600	602	605	601	604
10	425	432	436	457	823	503	463	753	733
14.2	202	197	205	200	370	-	222	401	400
15	-	-	-	-	-	253	-	-	-
20	102	104	118	105	130	160	144	225	214
25	68	69	74	68	85	101	105	151	150
30	55	52	56	58	62	77	82	111	110
40	35.5	36	34	-	44	54	64	76	72
50	25.1	24.6	26	25	33	41	47	55	52
65	16	16	18	12.2	23	30	32	37	37
80	13.5	13.5	14	13	20	25	25	31	28

^aTest numbers.

Table 7
 RADIATED KINETIC ENERGY IN INDIANA LIMESTONE (J)

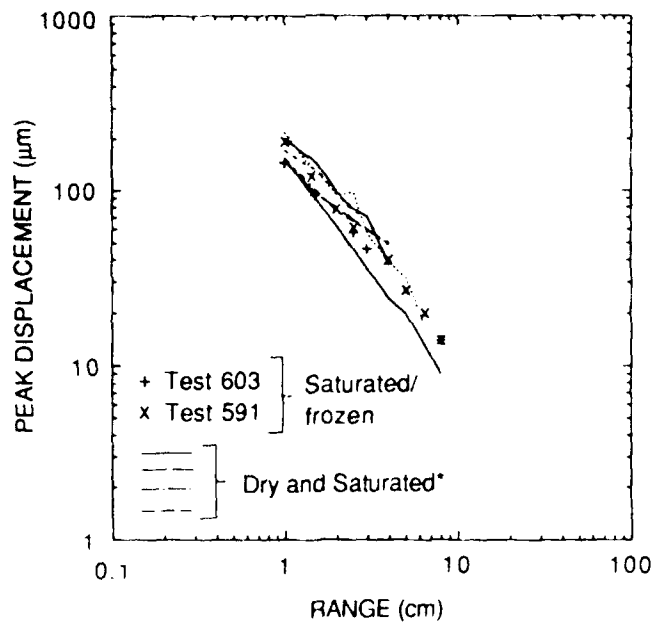
Range (mm)	Dry (Test 598)	Saturated (Test 601)	Saturated/Frozen (Test 602)
25	39	148	154
30	34	131	140
40	37	123	130
50	34	120	127
Average	36	131	138



*Data from Ref. 7

CM-1676-58

Figure 29. Comparison of velocity attenuation in Sierra White granite with different pore conditions.



*Data from Ref. 7

CM 1676 59

Figure 30. Comparison of displacement attenuation in Sierra White granite with different pore conditions.

Table 8
**MAXIMUM PARTICLE VELOCITIES IN
 SIERRA WHITE GRANITE (m/s)**

Range (mm)	Frozen Saturated			R.T. Saturated	R.T. Dry
	590 ^a	591	603	563	564
10	147	146	113	150	158
14.2	79	98	-	-	-
15	-	-	104	104	108
20	63	64	-	76	81
25	44	50	57	62	58
30	37	-	55	52	55
40	30	27	-	27	28
50	20	16	-	-	22
65	11.6	9.8	-	-	22
80	10.8	9.6	8	-	-

^aTest numbers.

Table 9

MAXIMUM DISPLACEMENTS IN
SIERRA WHITE GRANITE (μ/m)

Range (mm)	Frozen Saturated			R.T. Saturated	R.T. Dry
	590 ^a	591	603	563	564
10	264	192	144	200	171
14.2	156	120	-	-	-
15	-	-	93	147	132
20	108	78	-	104	96
25	75	61	57	78	75
30	65	-	47	71	70
40	46	39	-	38	37
50	34	28	-	-	32
65	26	20	-	-	-
80	18	14	14	-	-

^aTest numbers.

SECTION 5

CONCLUSIONS AND RECOMMENDATIONS

The experimental results showed that freezing affected the spherical waves only in the Indiana limestone in a saturated condition. The main effects on the wave characteristics caused by freezing of the saturated Indiana limestone are as follows:

- (1) The wave speed increased from 4.7 mm/ μ s to 5.6 mm/ μ s.
- (2) The peak particle velocity decreased by about 10%, the outward and inward velocity phases shortened by about 30%, and a precursor wave appeared at the short ranges.
- (3) The maximum and final radial displacements were reduced by about 30%.
- (4) The reduced velocity potential maintained its maximum value, but the phase was reduced by about 30%.
- (5) The reduced displacement potential decreased by about 50%.
- (6) The low frequency content of the velocity spectrum decreased by about a factor of 2. The corner frequency increased (30 to 50 kHz) and the decay of the high frequency content showed little change. Similar changes occurred for the spectra of the displacements and potentials.
- (7) The radiated kinetic energy remained the same.

The strong influence of freezing on the waves in saturated Indiana limestone is not surprising because the 16% porosity of our specimens was in the upper part of the range associated with limestone (1% to 22%). In Sierra White granite, however, the low porosity of 0.8% is insufficient to allow saturation at room temperature or frozen conditions to have an effect on wave propagation near the explosive source. We recommend that similar experiments be performed in limestone of lower porosity to determine the trend of the influence and possibly to be more representative of the rock at Novaya Zemlya.

REFERENCES

1. H. C. Heard, A. E. Abey, and B. P. Bonner, "High Pressure Mechanical Properties of Indiana Limestone," Lawrence Livermore National Laboratory Report UCID-16501, 11 June 1974.
2. S. E. Blouin and D. E. Chitty, "Strength and Deformation Properties of Salem Limestone," Applied Research Associates, Inc., Presentation at Defense Nuclear Agency Material Modeling Meeting at RDA, Marina del Rey, CA, Contract DNA 001-86-C-0149, 16 November 1988.
3. M. L. Green and J. S. Zelasko, "Material Property Tests on SRI Salem Limestone," U.S. Army Engineer Waterways Experiment Station Presentation at Defense Nuclear Agency Ground Shock Environmental Definition Meeting at CRT, Chatsworth, CA, 31 July 1991.
4. J. S. Zelasko, "High Strain Rate Properties for Salem Limestone Calculations," U.S. Army Engineer Waterways Experiment Station Presentation at Defense Nuclear Agency Range-to-Effect Meeting at RDA, Albuquerque, NM, 28 August 1990.
5. R. J. Martin III, K. B. Coyner, and R. W. Haupf, "Physical Properties Measurements on Analog Granites Related to the Joint Verification Experiment," New England Research, Inc., Report GL-TR-90-0171, 15 August 1990. ADA230571
6. P. R. Gefken, S. A. Miller, and A. L. Florence, "Spherical Waves in Jointed Limestone," SRI Bimonthly Progress Report No. 6 to the Defense Nuclear Agency (DNA), September 1991.
7. S. A. Miller and A. L. Florence, "Laboratory Particle Velocity Experiments on (JVE) Analog Rock," SRI Report GL-TR-90-0279(I), October 1990. ADA231894

APPENDIX A

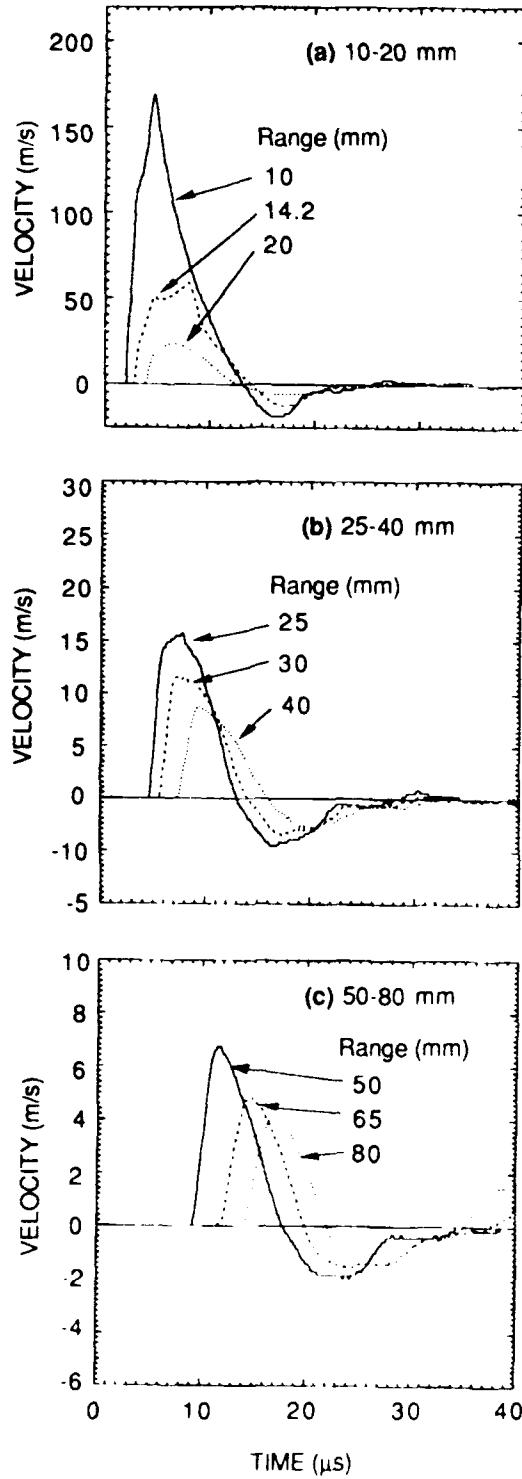
OTHER EXPERIMENTAL RESULTS

In Sections 2 and 3, we presented and compared results for the frozen/dry and frozen/saturated Indiana limestone Tests 598 and 602 and the frozen/saturated Sierra White granite Test 591 (Table 3). Here, we present particle velocity results for the repeat frozen/saturated Indiana limestone Tests 600 and 605; a direct comparison of the velocities at the 30-mm range for Tests 600, 602, and 605; and some displacement comparisons for Tests 602 and 605. We also present the particle velocity results for the frozen/saturated Sierra White granite Test 603 for comparison with the repeat Test 602.

Figures A1 and A2 show the particle velocities at the nine ranges in each of Tests 600 and 605 for frozen/saturated Indiana limestone. The overall forms are similar to each other and to those of Test 598 (Figure 2). The main differences are illustrated in Figure A3, which shows the particle velocities for the three tests at a range of 30 mm. Scatter exists primarily in the magnitudes of the outward and inward velocities. Test 600 exhibits more attenuation, which may be a result of incomplete filling of the pores with ice. For Tests 602 and 605, we used an improved freezing technique which included accurate weighings when the specimen was dry, saturated, and frozen (including the weight of water forced out under freezing pressures). The technique improved the reproducibility except for the magnitude of the rebound velocity.

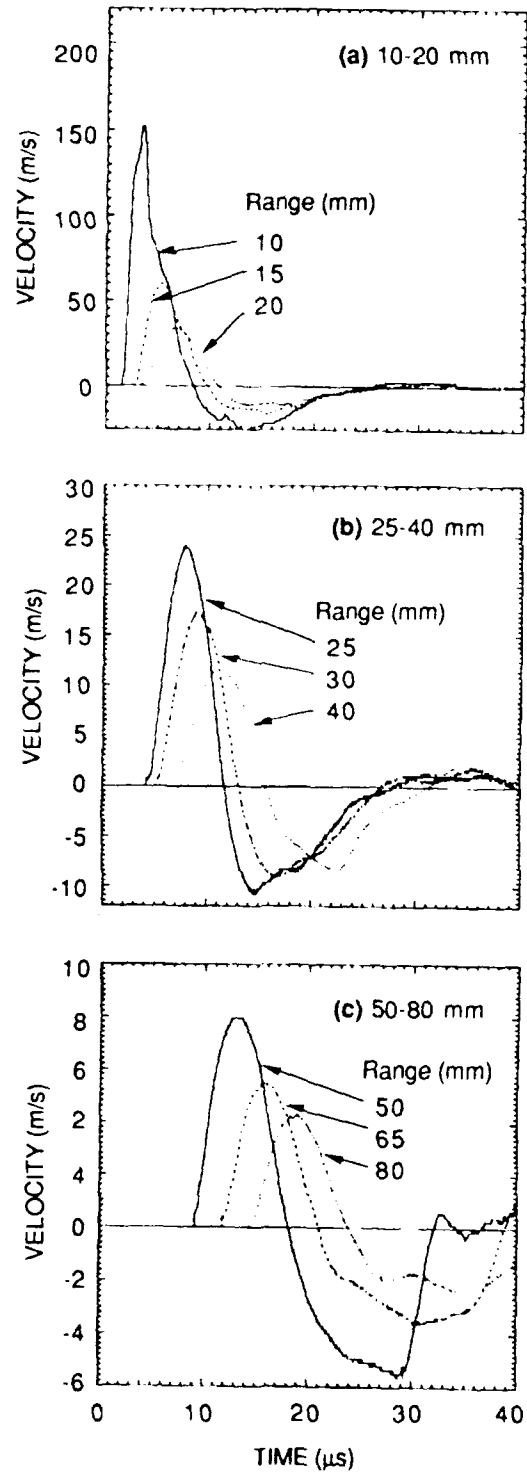
Figure A4 shows the displacements obtained at all ranges in Tests 602 and 605. Reproducibility is satisfactory except for the late-time portions of the outer ranges ($r > 20$ mm) where the larger rebound in Test 605 causes smaller final displacements.

Figure A5 compares particle velocity records in the frozen/saturated Sierra White granite Tests 591 and 603. Reproducibility is satisfactory. The records are basically the same as those of Tests 564 and 563 for dry and saturated Sierra White granite at room temperature.



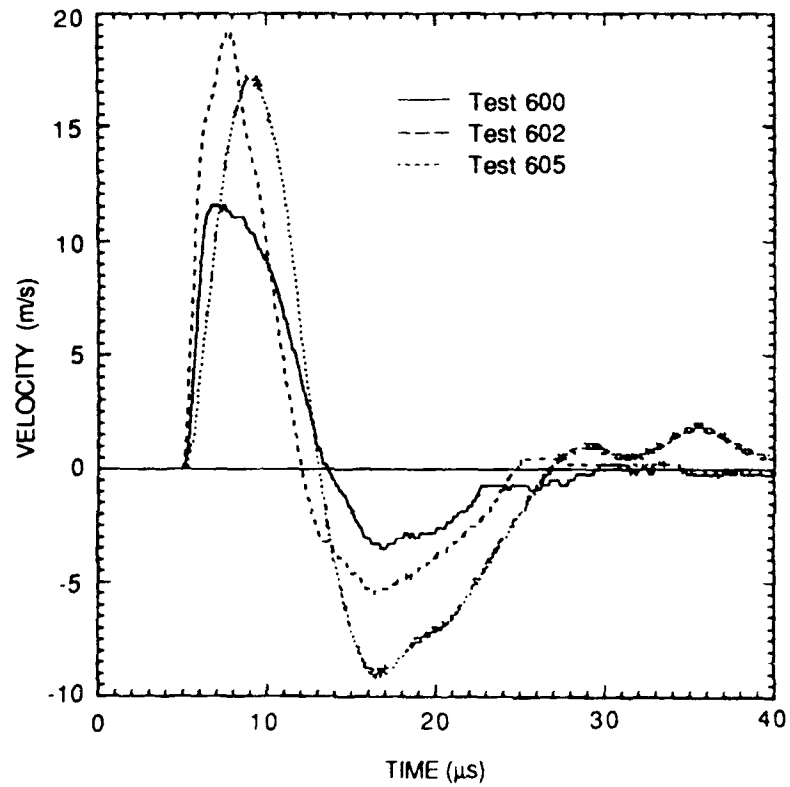
CM 1676 53

Figure A1. Particle velocity histories measured at nine ranges in saturated/frozen Indiana limestone, Test 600.



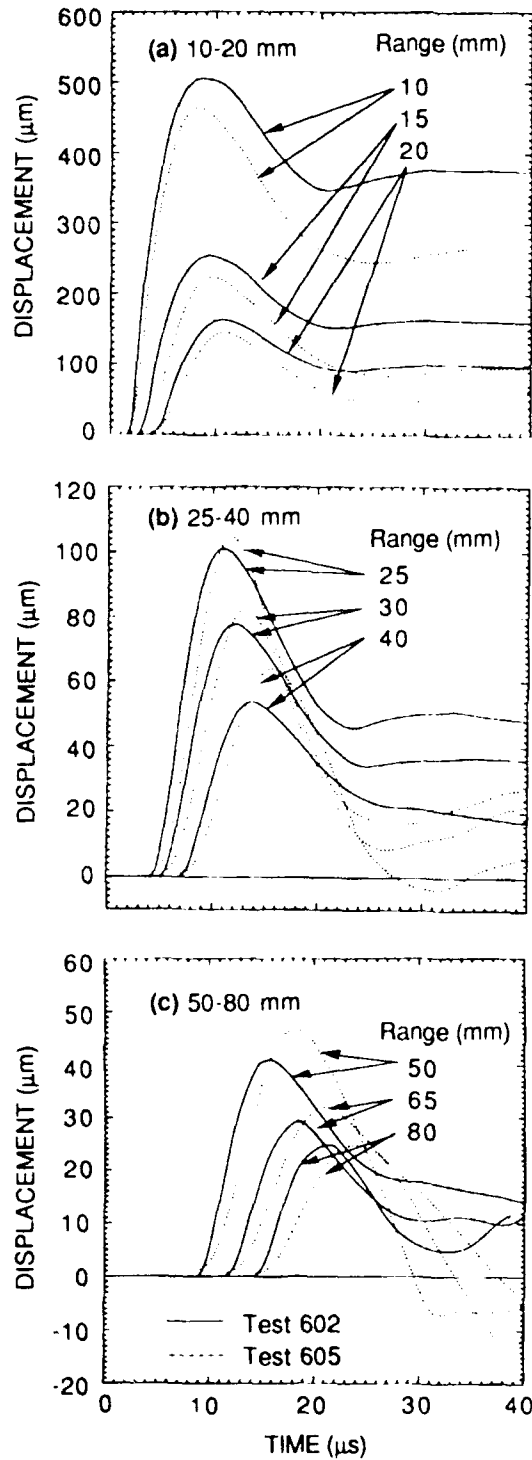
CM-1676-54

Figure A2. Particle velocity histories measured at nine ranges in saturated/frozen Indiana limestone, Test 605.



CM-1676-55

Figure A3. Comparison of velocity histories at 30-mm range in three experiments in saturated/frozen Indiana limestone.



CM-1676-56

Figure A4. Comparison of displacements at nine ranges from two experiments in saturated/frozen Indiana limestone.

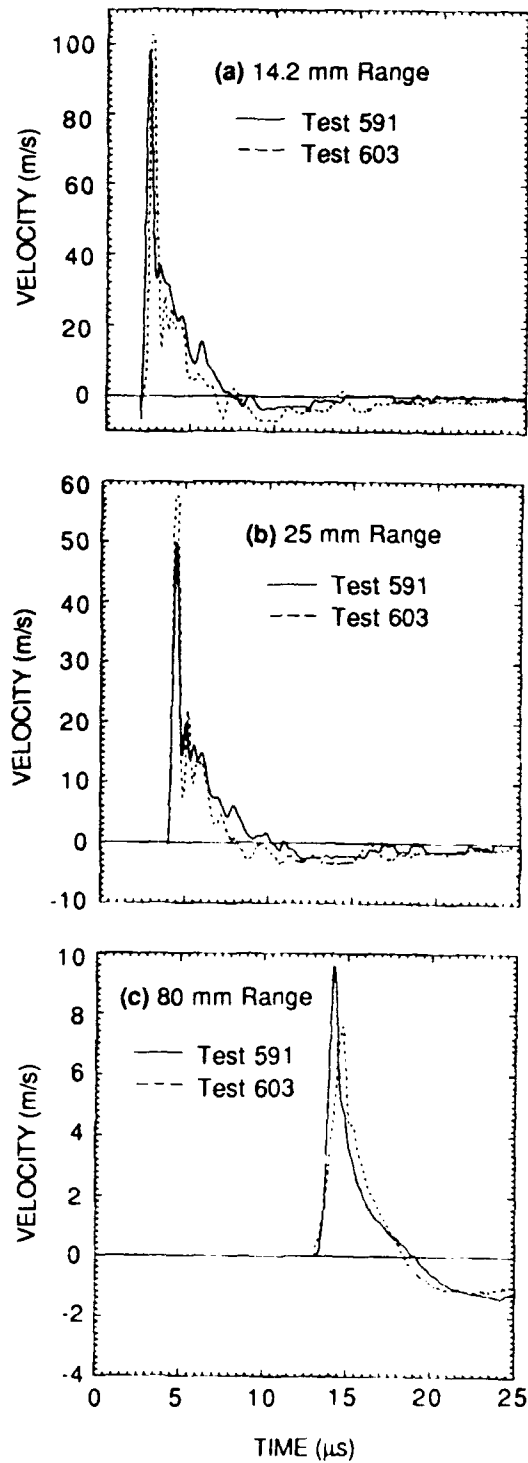


Figure A5. Comparison of velocity histories at different ranges from two experiments in saturated/frozen Sierra White granite.

APPENDIX B
DEFINITIONS AND FORMULAS

We have collected here definitions and formulas that we have employed for describing and interpreting the results.

With ξ and u representing the particle displacement and velocity in a spherical elastic wave, they can be expressed in terms of the RDP, ψ , and the RVP, γ , by

$$\xi = \frac{\partial}{\partial r} \left\{ -\frac{1}{r} \psi(\tau) \right\} \quad u = \frac{\partial}{\partial r} \left\{ -\frac{1}{r} \gamma(\tau) \right\} \quad \tau = t - (r - a)/c_p \quad (B1)$$

where τ is the time following arrival of the wave at the particle at range r and c_p is the P wave velocity.

The spectrum of discrete data $f(t_\alpha)$ at times t_α is provided by the Fourier transform $\tilde{f}(\omega_n)$ in the form

$$\tilde{f}(\omega_n) = c_n T = \frac{T}{N} \sum_{\alpha=0}^{N-1} f(t_\alpha) e^{-i\omega_n t_\alpha} \quad n = 0, 1, 2, \dots, N-1 \quad (B2)$$

in which c_n is the discrete Fourier transform, T is the time interval of the data measured from wave arrival, and ω_n is the n th angular frequency; the frequency is $\vartheta_n = \omega_n/2\pi = n/T$. From (B2)

$$|\tilde{f}| = |c_n| T = \left(a_n^2 + b_n^2 \right)^{1/2} T$$

where

$$a_n = \frac{1}{N} \sum_{\alpha=0}^{N-1} f_\alpha \cos \omega_n t_\alpha \quad b_n = \frac{1}{N} \sum_{\alpha=0}^{N-1} f_\alpha \sin \omega_n t_\alpha \quad (B3)$$

The radiated kinetic energy was calculated by means of

$$K(r) = 4\pi\rho c_p r^2 \int_0^T \left\{ u - (\xi - \psi/r^2)c_p/r \right\}^2 d\tau \quad (B4)$$

in which ρ is the material density.

Prof. Thomas Ahrens
Seismological Lab. 252-21
Division of Geological & Planetary Sciences
California Institute of Technology
Pasadena, CA 91125

Prof. Keiiti Aki
Center for Earth Sciences
University of Southern California
University Park
Los Angeles, CA 90089-0741

Prof. Shelton Alexander
Geosciences Department
403 Deike Building
The Pennsylvania State University
University Park, PA 16802

Dr. Ralph Alewine, III
DARPA/NMRO
3701 North Fairfax Drive
Arlington, VA 22203-1714

Prof. Charles B. Archambeau
CIRES
University of Colorado
Boulder, CO 80309

Dr. Thomas C. Bache, Jr.
Science Applications Int'l Corp.
10260 Campus Point Drive
San Diego, CA 92121 (2 copies)

Prof. Muawia Barazangi
Institute for the Study of the Continent
Cornell University
Ithaca, NY 14853

Dr. Jeff Barker
Department of Geological Sciences
State University of New York
at Binghamton
Vestal, NY 13901

Dr. Douglas R. Baumgardt
ENSCO, Inc
5400 Port Royal Road
Springfield, VA 22151-2388

Dr. Susan Beck
Department of Geosciences
Building #77
University of Arizona
Tucson, AZ 85721

Dr. T.J. Bennett
S-CUBED
A Division of Maxwell Laboratories
11800 Sunrise Valley Drive, Suite 1212
Reston, VA 22091

Dr. Robert Blandford
AFTAC/IT, Center for Seismic Studies
1300 North 17th Street
Suite 1450
Arlington, VA 22209-2308

Dr. G.A. Bollinger
Department of Geological Sciences
Virginia Polytechnical Institute
21044 Derring Hall
Blacksburg, VA 24061

Dr. Stephen Bratt
Center for Seismic Studies
1300 North 17th Street
Suite 1450
Arlington, VA 22209-2308

Dr. Lawrence Burdick
Woodward-Clyde Consultants
566 El Dorado Street
Pasadena, CA 91109-3245

Dr. Robert Burridge
Schlumberger-Doll Research Center
Old Quarry Road
Ridgefield, CT 06877

Dr. Jerry Carter
Center for Seismic Studies
1300 North 17th Street
Suite 1450
Arlington, VA 22209-2308

Dr. Eric Chael
Division 9241
Sandia Laboratory
Albuquerque, NM 87185

Prof. Vernon F. Cormier
Department of Geology & Geophysics
U-45, Room 207
University of Connecticut
Storrs, CT 06268

Prof. Steven Day
Department of Geological Sciences
San Diego State University
San Diego, CA 92182

Marvin Denny
U.S. Department of Energy
Office of Arms Control
Washington, DC 20585

Dr. Zoltan Der
ENSCO, Inc.
5400 Port Royal Road
Springfield, VA 22151-2388

Prof. Adam Dziewonski
Hoffman Laboratory, Harvard University
Dept. of Earth Atmos. & Planetary Sciences
20 Oxford Street
Cambridge, MA 02138

Prof. John Ebel
Department of Geology & Geophysics
Boston College
Chestnut Hill, MA 02167

Eric Fielding
SNEE Hall
INSTOC
Cornell University
Ithaca, NY 14853

Dr. Mark D. Fisk
Mission Research Corporation
735 State Street
P.O. Drawer 719
Santa Barbara, CA 93102

Prof Stanley Flatte
Applied Sciences Building
University of California, Santa Cruz
Santa Cruz, CA 95064

Dr. John Foley
NER-Geo Sciences
1100 Crown Colony Drive
Quincy, MA 02169

Prof. Donald Forsyth
Department of Geological Sciences
Brown University
Providence, RI 02912

Dr. Art Frankel
U.S. Geological Survey
922 National Center
Reston, VA 22092

Dr. Cliff Frolich
Institute of Geophysics
8701 North Mopac
Austin, TX 78759

Dr. Holly Given
IGPP, A-025
Scripps Institute of Oceanography
University of California, San Diego
La Jolla, CA 92093

Dr. Jeffrey W. Given
SAIC
10260 Campus Point Drive
San Diego, CA 92121

Dr. Dale Glover
Defense Intelligence Agency
ATTN: ODT-1B
Washington, DC 20301

Dr. Indra Gupta
Teledyne Geotech
314 Montgomery Street
Alexandria, VA 22314

Dan N. Hagedorn
Pacific Northwest Laboratories
Battelle Boulevard
Richland, WA 99352

Dr. James Hannon
Lawrence Livermore National Laboratory
P.O. Box 808
L-205
Livermore, CA 94550

Dr. Roger Hansen
HQ AFTAC/TTR
Patrick AFB, FL 32925-6001

Prof. David G. Harkrider
Seismological Laboratory
Division of Geological & Planetary Sciences
California Institute of Technology
Pasadena, CA 91125

Prof. Danny Harvey
CIRES
University of Colorado
Boulder, CO 80309

Prof. Donald V. Helmberger
Seismological Laboratory
Division of Geological & Planetary Sciences
California Institute of Technology
Pasadena, CA 91125

Prof. Eugene Herrin
Institute for the Study of Earth and Man
Geophysical Laboratory
Southern Methodist University
Dallas, TX 75275

Prof. Robert B. Herrmann
Department of Earth & Atmospheric Sciences
St. Louis University
St. Louis, MO 63156

Prof. Lane R. Johnson
Seismographic Station
University of California
Berkeley, CA 94720

Prof. Thomas H. Jordan
Department of Earth, Atmospheric &
Planetary Sciences
Massachusetts Institute of Technology
Cambridge, MA 02139

Prof. Alan Kafka
Department of Geology & Geophysics
Boston College
Chestnut Hill, MA 02167

Robert C. Kemerait
ENSCO, Inc.
445 Pineda Court
Melbourne, FL 32940

Dr. Max Koontz
U.S. Dept. of Energy/DP 5
Forrestal Building
1000 Independence Avenue
Washington, DC 20585

Dr. Richard LaCoss
MIT Lincoln Laboratory, M-200B
P.O. Box 73
Lexington, MA 02173-0073

Dr. Fred K. Lamb
University of Illinois at Urbana-Champaign
Department of Physics
1110 West Green Street
Urbana, IL 61801

Prof. Charles A. Langston
Geosciences Department
403 Deike Building
The Pennsylvania State University
University Park, PA 16802

Jim Lawson, Chief Geophysicist
Oklahoma Geological Survey
Oklahoma Geophysical Observatory
P.O. Box 8
Leonard, OK 74043-0008

Prof. Thorne Lay
Institute of Tectonics
Earth Science Board
University of California, Santa Cruz
Santa Cruz, CA 95064

Dr. William Leith
U.S. Geological Survey
Mail Stop 928
Reston, VA 22092

Mr. James F. Lewkowicz
Phillips Laboratory/GPEH
Hanscom AFB, MA 01731-5000(2 copies)

Mr. Alfred Lieberman
ACDA/VI-OA State Department Building
Room 5726
320-21st Street, NW
Washington, DC 20451

Prof. L. Timothy Long
School of Geophysical Sciences
Georgia Institute of Technology
Atlanta, GA 30332

Dr. Randolph Martin, III
New England Research, Inc.
76 Olcott Drive
White River Junction, VT 05001

Dr. Robert Masse
Denver Federal Building
Box 25046, Mail Stop 967
Denver, CO 80225

Dr. Gary McCartor
Department of Physics
Southern Methodist University
Dallas, TX 75275

Prof. Thomas V. McEvilly
Seismographic Station
University of California
Berkeley, CA 94720

Dr. Art McGarr
U.S. Geological Survey
Mail Stop 977
U.S. Geological Survey
Menlo Park, CA 94025

Dr. Keith L. McLaughlin
S-CUBED
A Division of Maxwell Laboratory
P.O. Box 1620
La Jolla, CA 92038-1620

Stephen Miller & Dr. Alexander Florence
SRI International
333 Ravenswood Avenue
Box AF 116
Menlo Park, CA 94025-3493

Prof. Bernard Minster
IGPP, A-025
Scripps Institute of Oceanography
University of California, San Diego
La Jolla, CA 92093

Prof. Brian J. Mitchell
Department of Earth & Atmospheric Sciences
St. Louis University
St. Louis, MO 63156

Mr. Jack Murphy
S-CUBED
A Division of Maxwell Laboratory
11800 Sunrise Valley Drive, Suite 1212
Reston, VA 22091 (2 Copies)

Dr. Keith K. Nakanishi
Lawrence Livermore National Laboratory
L-025
P.O. Box 808
Livermore, CA 94550

Dr. Carl Newton
Los Alamos National Laboratory
P.O. Box 1663
Mail Stop C335, Group ESS-3
Los Alamos, NM 87545

Dr. Bao Nguyen
HQ AFTAC/TTR
Patrick AFB, FL 32925-6001

Prof. John A. Orcutt
IGPP, A-025
Scripps Institute of Oceanography
University of California, San Diego
La Jolla, CA 92093

Prof. Jeffrey Park
Kline Geology Laboratory
P.O. Box 6666
New Haven, CT 06511-8130

Dr. Howard Patton
Lawrence Livermore National Laboratory
L-025
P.O. Box 808
Livermore, CA 94550

Dr. Frank Pilotte
HQ AFTAC/TT
Patrick AFB, FL 32925-6001

Dr. Jay J. Pulli
Radix Systems, Inc.
2 Taft Court, Suite 203
Rockville, MD 20850

Dr. Robert Reinke
ATTN: FCTVTD
Field Command
Defense Nuclear Agency
Kirtland AFB, NM 87115

Prof. Paul G. Richards
Lamont-Doherty Geological Observatory
of Columbia University
Palisades, NY 10964

Mr. Wilmer Rivers
Teledyne Geotech
314 Montgomery Street
Alexandria, VA 22314

Dr. George Rothe
HQ AFTAC/TTR
Patrick AFB, FL 32925-6001

Dr. Alan S. Ryall, Jr.
DARPA/NMRO
3701 North Fairfax Drive
Arlington, VA 22209-1714

Dr. Richard Sailor
TASC, Inc.
55 Walkers Brook Drive
Reading, MA 01867

Prof. Charles G. Sammis
Center for Earth Sciences
University of Southern California
University Park
Los Angeles, CA 90089-0741

Prof. Christopher H. Scholz
Lamont-Doherty Geological Observatory
of Columbia University
Palisades, CA 10964

Dr. Susan Schwartz
Institute of Tectonics
1156 High Street
Santa Cruz, CA 95064

Secretary of the Air Force
(SAFRD)
Washington, DC 20330

Office of the Secretary of Defense
DDR&E
Washington, DC 20330

Thomas J. Sereno, Jr.
Science Application Int'l Corp.
10260 Campus Point Drive
San Diego, CA 92121

Dr. Michael Shore
Defense Nuclear Agency/SPSS
6801 Telegraph Road
Alexandria, VA 22310

Dr. Matthew Sibol
Virginia Tech
Seismological Observatory
4044 Derring Hall
Blacksburg, VA 24061-0420

Prof. David G. Simpson
IRIS, Inc.
1616 North Fort Myer Drive
Suite 1440
Arlington, VA 22209

Donald L. Springer
Lawrence Livermore National Laboratory
L-025
P.O. Box 808
Livermore, CA 94550

Dr. Jeffrey Stevens
S-CUBED
A Division of Maxwell Laboratory
P.O. Box 1620
La Jolla, CA 92038-1620

Lt. Col. Jim Stobie
ATTN: AFOSR/NL
Bolling AFB
Washington, DC 20332-6448

Prof. Brian Stump
Institute for the Study of Earth & Man
Geophysical Laboratory
Southern Methodist University
Dallas, TX 75275

Prof. Jeremiah Sullivan
University of Illinois at Urbana-Champaign
Department of Physics
1110 West Green Street
Urbana, IL 61801

Prof. L. Sykes
Lamont-Doherty Geological Observatory
of Columbia University
Palisades, NY 10964

Dr. David Taylor
ENSCO, Inc.
445 Pineda Court
Melbourne, FL 32940

Dr. Steven R. Taylor
Los Alamos National Laboratory
P.O. Box 1663
Mail Stop C335
Los Alamos, NM 87545

Prof. Clifford Thurber
University of Wisconsin-Madison
Department of Geology & Geophysics
1215 West Dayton Street
Madison, WI 53706

Prof. M. Nafi Toksoz
Earth Resources Lab
Massachusetts Institute of Technology
42 Carleton Street
Cambridge, MA 02142

Dr. Larry Turnbull
CIA-OSWR/NED
Washington, DC 20505

DARPA/RMO/SECURITY OFFICE
3701 North Fairfax Drive
Arlington, VA 22203-1714

Dr. Gregory van der Vink
IRIS, Inc.
1616 North Fort Myer Drive
Suite 1440
Arlington, VA 22209

HQ DNA
ATTN: Technical Library
Washington, DC 20305

Dr. Karl Veith
EG&G
5211 Auth Road
Suite 240
Suitland, MD 20746

Defense Intelligence Agency
Directorate for Scientific & Technical Intelligence
ATTN: DTIB
Washington, DC 20340-6158

Prof. Terry C. Wallace
Department of Geosciences
Building #77
University of Arizona
Tucson, AZ 85721

Defense Technical Information Center
Cameron Station
Alexandria, VA 22314 (2 Copies)

Dr. Thomas Weaver
Los Alamos National Laboratory
P.O. Box 1663
Mail Stop C335
Los Alamos, NM 87545

TACTEC
Battelle Memorial Institute
505 King Avenue
Columbus, OH 43201 (Final Report)

Dr. William Wor man
Mission Research Corporation
8560 Cinderbed Road
Suite 700
Newington, VA 22122

Phillips Laboratory
ATTN: XPG
Hanscom AFB, MA 01731-5000

Prof. Francis T. Wu
Department of Geological Sciences
State University of New York
at Binghamton
Vestal, NY 13901

Phillips Laboratory
ATTN: GPE
Hanscom AFB, MA 01731-5000

AFTAC/CA
(STINFO)
Patrick AFB, FL 32925-6001

Phillips Laboratory
ATTN: TSML
Hanscom AFB, MA 01731-5000

DARPA/PM
3701 North Fairfax Drive
Arlington, VA 22203-1714

Phillips Laboratory
ATTN: SUL
Kirtland, NM 87117 (2 copies)

DARPA/RMO/RETRIEVAL
3701 North Fairfax Drive
Arlington, VA 22203-1714

Dr. Michel Bouchon
I.R.I.G.M.-B.P. 68
38402 St. Martin D'Herès
Cedex, FRANCE

Dr. Michel Campillo
Observatoire de Grenoble
I.R.I.G.M.-B.P. 53
38041 Grenoble, FRANCE

Dr. Jorg Schlittenhardt
Federal Institute for Geosciences & Nat'l Res.
Postfach 510153
D-3000 Hannover 51, GERMANY

Dr. Kin Yip Chun
Geophysics Division
Physics Department
University of Toronto
Ontario, CANADA

Dr. Johannes Schweitzer
Institute of Geophysics
Ruhr University/Bochum
P.O. Box 1102148
4360 Bochum 1, GERMANY

Prof. Hans-Peter Harjes
Institute for Geophysic
Ruhr University/Bochum
P.O. Box 102148
4630 Bochum 1, GERMANY

Prof. Eystein Husebye
NTNF/NORSAR
P.O. Box 51
N-2007 Kjeller, NORWAY

David Jepsen
Acting Head, Nuclear Monitoring Section
Bureau of Mineral Resources
Geology and Geophysics
G.P.O. Box 378, Canberra, AUSTRALIA

Ms. Eva Johannisson
Senior Research Officer
National Defense Research Inst.
P.O. Box 27322
S-102 54 Stockholm, SWEDEN

Dr. Peter Marshall
Procurement Executive
Ministry of Defense
Blacknest, Brimpton
Reading FG7-FRS, UNITED KINGDOM

Dr. Bernard Massinon, Dr. Pierre Mechler
Societe Radiomana
27 rue Claude Bernard
75005 Paris, FRANCE (2 Copies)

Dr. Svein Mykkeltveit
NTNF/NORSAR
P.O. Box 51
N-2007 Kjeller, NORWAY (3 Copies)

Prof. Keith Priestley
University of Cambridge
Bullard Labs, Dept. of Earth Sciences
Madingley Rise, Madingley Road
Cambridge CB3 0EZ, ENGLAND